NSG-1483

BUCKLING OF THERMOVISCOELASTIC STRUCTURES UNDER TEMPORAL AND SPATIAL TEMPERATURE VARIATIONS

by

Richard Tsuyuki
Orbital Sciences, Inc.

and

Wolfgang G. Knauss
Professor of Aeronautics and Applied Mechanics

California Institute of Technology
Pasadena, CA 91125

Abstract

The problem of lateral instability of a viscoelastic in-plane loaded structure is considered in terms of thermorheologically simple materials. As an example of a generally in-plane loaded structure, we examine the simple column under axial load: Both cyclic loading is considered (with constant or in-phase variable temperature excursions) as well as the case of constant load in the presence of thermal gradients through the thickness of the structure. The latter case involves a continuous movement of the neutral axis from the center to the colder side and then back to the center.

In both cases, temperature has a very strong effect on the instability evolution, and under in-phase thermal cycling the critical loads are reduced compared to those at constant temperatures. The primary effect of thermal gradients beyond that of thermally-induced rate accelerations is occasioned by the generation of an "initial imperfection" or "structural bowing." Because the coefficient of thermal expansion tends to be large for many polymeric materials, it may be necessary to take special care in lay-up design of composite structures intended for use under compressive loads in high-temperature applications. Finally, the implications for the temperature sensitivities of composites to micro-instability (fiber crimping) are also apparent from the results delineated here.

1. Introduction

Besides fracture, an important structural failure mode revolves around the evolution of unstable lateral deformations, often characterized as buckling. When time-dependent material behavior is involved, such as associated with polymer-based composites, this behavior depends strongly on the time history of loading and, even more so, on temperature. While one can always estimate from the relaxation or creep properties of the material lower-bound load values below which instabilities never arise [Drozdov], such bounds tend to be so low from a practical point of view that the designer is forced to use these materials at load levels at which instabilities *can* evolve eventually, but such that they develop on a time scale that is large compared to the anticipated life of the structure. Composites are typically used in their rigid or (near-)glassy state; it is then of interest to examine the variation in their response history as one deviates from typical low-temperature design conditions.

The problem of buckling in viscoelastic structures has been considered by several authors. Most of these deal with response under constant axial or in-plane loads. Closely attuned to the present objective, Schapery has examined the cyclic loading of viscoelastic columns under constant temperature. We shall emphasize in the present study, as did Schapery,

realistically wide time ranges of material response rather than idealized behavior. However, the present effort focuses on the derivation of stability criteria and the effect of time-varying temperature cycles.

The large time-range for buckling evolution follows from the large range of time-dependence of polymers, even when they are married to rate-insensitive reinforcements such as graphite fibers. The "stiffness" of polymers drops by a factor of 10^2 to 10^3 with time or temperature increase as the glass-transition temperature is traversed. Under these circumstances it is imperative that one appreciate the limitations placed on structures by operation at elevated temperatures. While it is obviously inappropriate to allow the use of these materials uniformly at or above the glass transition, the possibility exists that they are exposed to temperature gradients in which part of the material experiences near-transition temperatures, or situations may arise when such temperatures are accidentally approached or exceeded.

With this motivation in mind we examine columns possessing thermorheologically simple material behavior subjected to two kinds of (axial) loading and thermal exposure: We consider first the case of a cyclically loaded column under constant as well as cyclically varying temperature, the latter being in phase with the loading. This problem will be first considered for the idealized material of a standard linear solid to establish certain limit behaviors. This simplified-material and exact analysis is then followed by a numerical evaluation involving realistically wide-spectrum time response following the behavior of polymethylmethacrylate (PMMA) as a model material. Along the length of the column the temperature distribution is presumed constant for all problems considered here.

The next problem concerns the effect of a thermal gradient across the thickness of the structure. Mimicking steady-state thermal conditions we consider only a linear temperature variation across the column (although a different distribution poses no additional difficulty in principle). The consequence of this thermal variation is that with time the material exhibits varying "stiffness" across the structure, since higher temperatures are associated with faster relaxation or creep, so that the neutral axis (surface) wanders as time progresses: While being located initially and also after infinite time at the center, it is subject to an intermediate excursion towards the cold side.

Problems of time-dependent buckling instability in the absence of temperature gradients have been considered by other authors. We believe that a fair review of the state of the art in this respect is presented in the references by Glockner and Szyszkowski (1987) and Minahen and Knauss (1992). For our present purposes it suffices to state that in the context of the time-dependent, non-dynamic evolution of instabilities, the criterion as to when unsafe conditions have been achieved must be established through empirical arguments; in this regard we follow Minahen and Knauss (1992) and use the achievement of a predetermined lateral deflection as the criterion for failure. Also, in view of the results

in this latter reference, namely that considerations of kinematically large deformations yield virtually identical results as the completely linearized analysis, we restrict ourselves here also to linear kinematics and material response.

2. General Formulation

Following developments in Minahen and Knauss (1992) we consider an initially (slightly) deformed column, as shown in figure 1, of in-plane thickness h and unit out-of-plane thickness. In anticipation of dealing with thermal gradients through the thickness and the associated motion of the neutral axis, we designate that position with respect to the center-line as $n(t)$. Let $u_0(x,t)$ denote the axial motion of the center-line, α_x the (constant) coefficient of linear thermal expansion, and $T(z,t)$ the temperature variation. The strain is then

$$\epsilon_x(z,t) = \frac{\partial u_0}{\partial x}(t) - [z - n(t)]\frac{\partial^2 w}{\partial x^2} + \alpha_x T(z) \tag{1}$$

along with the stress-strain relation

$$\sigma_x(z,t) = \int_{-\infty}^{t} E(z, t' - \xi')\,\frac{\partial}{\partial \xi}\epsilon_x(z,\xi)\,d\xi \tag{2}$$

where

$$t' - \xi' = \int_{\xi}^{t} \frac{d\zeta}{\phi[T(z,\zeta)]} \tag{3}$$

is the reduced time (difference) based on the time-temperature shift factor $\phi(T)$. Moment equilibrium then provides the integro-differential equation

$$\int_{-\frac{h}{2}}^{\frac{h}{2}} [z - n(t)] \int_{-\infty}^{t} E(z, t' - \xi')\frac{\partial}{\partial \xi}\left\{\frac{\partial u_0}{\partial x}(\xi) - [z - n(\xi)]\frac{\partial^2 w}{\partial x^2}\right\} d\xi\, dz = P\,[w(x,t) + w_0(x) + n(t)] \tag{4}$$

with $w_o(x)$ and $w(x,t)$ denoting, respectively, the small initial imperfection (when needed) and the additional time-dependent lateral deflection as illustrated in figure 1. After expanding $w_0(x)$ and $w(x,t)$ into the Fourier series

$$w(x,t) = \sum_{m=1}^{\infty} A_m(t) \sin\frac{m\pi x}{l} \tag{5}$$

and

$$w_0(x) = \sum_{m=1}^{\infty} B_m \sin\frac{m\pi x}{l} \tag{6}$$

two equations result, one governing the location of the neutral axis

$$\int_{-\frac{h}{2}}^{\frac{h}{2}} [z - n(t)] \int_{-\infty}^{t} E(z, t' - \xi')\frac{\partial}{\partial \xi}\left[\frac{\partial u_0}{\partial x}(\xi)\right] d\xi\, dz = P\, n(t) \tag{7}$$

and the other representing moment equilibrium

$$\left(\frac{\pi}{l}\right)^2 \int_{-\frac{h}{2}}^{\frac{h}{2}} [z - n(t)] \int_{-\infty}^{t} E(z, t' - \xi') \frac{\partial}{\partial \xi} \{[z - n(\xi)] A(\xi)\} \, d\xi \, dz = P\,[A(t) + B] \quad (8)$$

where, in anticipation of dealing only with the fundamental mode ($m = 1$) [see Minahen and Knauss (1992)], the subscripts m have been dropped. [1] Because the two problems to be considered subsequently need a somewhat different use of the last two equations, we shall deal with their applications in the specific contexts.

3. Cyclic Loading

Before dealing with a material possessing realistic time response, we consider first the case of the standard linear solid with the intention of characterizing the typical aspects of the problem and to allow for an evaluation of the numerical scheme applied later to the situation with more realistic properties. Computational solutions require compromises in the discretization of the integration so that a check on the reliability of the scheme is at least desirable, if not mandatory, in light of earlier experience in Minahen and Knauss (1992). We choose a "square wave" loading history because it approximates typical use conditions better than a sinusoidal history, but also with the expectation that a piece-wise sequential solution is possible. The results obtained in the sequel for equal on/off times are readily generalized for unequal on/off ratios with square wave loading. The thermal excursions are of the same type so that a rise in load is accompanied by a rise in temperature and unloading is accompanied by a drop in temperature without considerations of thermal delay transients (c.f. figure 2). In fact, it turns out that any piecewise-constant load history can be dealt with using the procedure developed below, such that the effects of loading functions with multiple load levels or discretized approximations of load histories which do not resemble square waves can be obtained with only slightly more effort.

3.1.1 Standard linear solid; isothermal case

Because in the present case the temperature is uniform throughout the geometry, the neutral axis remains at the center-line or midsurface ($n \equiv 0$). Equation (7) is thus satisfied identically and, after normalizations in the form of

$$p(t) \equiv \frac{P(t)}{P_e(0)}, \quad P_e(t) \equiv \left(\frac{\pi}{l}\right)^2 E(t) I$$

$$r(t) \equiv \frac{E(t)}{E(0)}, \quad a(t) \equiv \frac{A(t)}{h}, \quad \beta \equiv \frac{B}{h} \quad (9)$$

[1] It was shown in the work of Minahen and Knauss that, generally, of all the possible deformation modes the first one grows significantly faster than the higher ones. For this reason the first mode will dominate the deformation evolution.

the moment equation (8) reduces to

$$r(t')\alpha(0^+) + \int_{0+}^{t} r(t'-\xi')\frac{d\alpha(\xi)}{d\xi}d\xi = p(t)[\alpha(t)+\beta] \tag{10}$$

For the standard linear solid, the relaxation behavior is characterized by

$$r(t) = r_\infty + r_1 e^{-\lambda t}; \quad r_\infty = \frac{E(\infty)}{E(0)}; \quad r_1 = 1 - r_\infty. \tag{11}$$

We effect a solution of (10) for a loading-unloading-loading cycle to show by induction that a sequential or recursive solution may be obtained. First integrate (10) across the load jump at $t = 0$ to obtain

$$\alpha(0^+) = \frac{p_0\beta}{1-p_0} \tag{12}$$

and then establish the lateral column motion under time-invariant axial loading. This result was given in Minahen and Knauss (1992) for any load level p_0 as shown in figure 3, which is valid for the first loading portion, with the explicit form for this function being given, for arbitrarily long pulse duration t, by

$$\alpha_{l1}(t) = C_1 e^{-\mu t} + C_2 \tag{13}$$

where

$$C_1 \equiv \alpha(0^+) + \frac{p_0\beta}{p_0 - r_\infty}, \quad \mu \equiv -\lambda\frac{p_0 - r_\infty}{1-p_0}, \quad C_2 \equiv -\frac{p_0\beta}{p_0 - r_\infty}. \tag{14}$$

We shall refer hereafter to (13) as the *deflection function*. Integrating (10) also across the unloading jump at $t = t_0$ yields the corresponding deflection decrease

$$\Delta\alpha = -p_0[\alpha(t_0^-) + \beta]. \tag{15}$$

To obtain the deflection for the unloaded portion of the cycle we let

$$p(t) = p_0[h(t) - h(t-t_0)] \tag{16}$$

in (10), and deduce, with the aid of Laplace transformation and some tedious algebra, that during the time $t_0 < t < 2t_0$ the lateral midspan deflection is

$$\alpha_{ul1}(t) = C_3 e^{-r_\infty \lambda t} \tag{17}$$

with

$$C_3 \equiv p_0[(C_2 + \beta)\frac{r_1}{r_\infty}(e^{r_\infty \lambda t_0} - 1) + \frac{C_1 r_1 \lambda}{\mu - r_\infty \lambda}(1 - e^{(r_\infty \lambda - \mu)t_0})]. \tag{18}$$

One follows the same procedure for the time interval $2t_0 < t < 3t_0$ and determines that during this second loading cycle,

$$\alpha_{l2}(t) = C_4 e^{-\mu t} + C_2 \tag{19}$$

where

$$C_4 = \alpha_0^+ \frac{1 - r_\infty}{p_0 - r_\infty}(1 - e^{\mu t_0} + e^{2\mu t_0}) + \frac{C_3}{1 - p_0}[e^{(\mu - r_\infty \lambda)t_0} - e^{2(\mu - r_\infty \lambda)t_0}] \tag{20}$$

μ and C_2 are the same as in (14), and C_3 is defined in (18). Comparison with (13) shows that this response can be determined from the deflection under step-loading in equation (13) through a "time shift" of the form

$$\alpha_{I2}(t) = C_1 e^{-\mu(t-\hat{t})} + C_2, \quad \hat{t} = \frac{1}{\mu} \ln \frac{C_4}{C_1} \tag{21}$$

which observation is also illustrated in figure 4. Because further stepwise integration becomes very cumbersome even for this simple material problem, we deduce by induction that a sequence for further load cycles may be constructed through successive determination of the (glassy) jumps at the loading and unloading times plus segments of the loading and unloading functions, (13) and (17) respectively, such that their magnitudes match the values at the beginnings or ends of the load cycles. [2] In this sense, these two curves become "master curves" for the deformation during the loaded and unloaded portions of the cycles.

3.1.2 Long-term stability

This term-by-term construction of the solution becomes tedious and because we are interested only in the maximum deflection at the end of each cycle we are satisfied with tracing the history of that particular parameter. To this end, we consider the accumulation of the deflection over a postulated load cycle by considering the jumps at the loading and unloading time nt_0 and $(n+1)t_0$, as well as the change during the respective time intervals. Starting with the deflection at the end of a loading cycle, $\alpha(nt_0^-)$, we find the subsequent (downward) jump

$$\alpha(nt_0^+) = \alpha(nt_0^-) - p_0[\alpha(nt_0^-) + \beta] \tag{22}$$

the displacement at the end of the unloaded interval

$$\alpha[(n+1)t_0^-] = \alpha(nt_0^+)e^{-r_\infty \lambda t_0} \tag{23}$$

the (upward) jump at the onset of a new loading interval

$$\alpha[(n+1)t_0^+] = \alpha[(n+1)t_0^-] + \frac{p_0[\alpha[(n+1)t_0^-] + \beta]}{1 - p_0} \tag{24}$$

[2] This response history has also been computed numerically for comparison purposes and as a check on the algorithm used later. With 100 or 1000 time steps per cycle it was found that over the duration of 40 cycles the differences amounted to no more than 0.1%. The same result prevailed for cycles possessing fractions of the loading/unloading cycle that differed from the 50/50 example illustrated here.

and the displacement at the end of the next loading interval

$$\alpha[(n+2)t_0^-] = [\alpha[(n+1)t_0^+] - C_2]e^{-\mu t_0} + C_2. \tag{25}$$

By combining (22) through (25) one finds

$$\Delta\alpha_{\text{cycle}} \equiv \alpha[(n+2)t_0^-] - \alpha(nt_0^-) \tag{26}\$$

and therefore

$$\Delta\alpha_{\text{cycle}} = [e^{-(r_\infty\lambda+\mu)t_0} - 1]\alpha(nt_0^-) + \alpha(0^+)(1 - e^{-r_\infty\lambda t_0})e^{-\mu t_0} + C_2(1 - e^{-\mu t_0}) \tag{27}$$

recalling that $\alpha(0^+)$ is given by equation (12).

It is apparent that the character of the accumulated deflections is determined by the term multiplying $\alpha(nt_0^-)$. If this term is negative, successive deflection increments decrease with time so that the total deflection tends asymptotically to an upper limit. It is negative if $(r_\infty\lambda + \mu) > 0$ which, with (14), indicates stability if

$$p_0 < p_{cr} \equiv \frac{2r_\infty}{1 + r_\infty} \tag{28}$$

in which case the maximum deflection is asymptotic (i.e., $\Delta\alpha_{\text{cycle}} = 0$) to

$$\alpha_{\max}(\infty) = \frac{\alpha(0^+)(1 - e^{-r_\infty\lambda t_0})e^{-\mu t_0} + C_2(1 - e^{-\mu t_0})}{1 - e^{-(r_\infty\lambda+\mu)t_0}}. \tag{29}$$

It is clear that if $p \geq p_{cr}$ a bounded displacement is not achieved as $t \to \infty$; in fact, if $p = p_{cr}$, the displacement amplitude diverges linearly with time or number of cycles, while it grows exponentially if $p > p_{cr}$. Illustrations of these three distinct cases are given in figures 5–7. For these examples the standard linear solid model used is

$$r(t) = 0.5(1 + e^{-(t/7.21\text{hrs})}). \tag{30}$$

3.1.3 Standard linear solid; in-phase thermal cycling

Because of the piecewise construction of the solution, the extension to thermal variations is simple, whether that variation is in-phase or out-of-phase. The situation for thermal cycling which is phase-shifted with respect to the loading by a fixed amount is only slightly more complicated than the case presented here, while the case of thermal cycling with a different frequency than the load cycle does not seem to lend itself to any other than a completely numerical solution. From an engineering point of view, the (approximately) synchronous load and temperature variation presents the most relevant problem and is the only one considered here.

We assume that for this simple material model, a time-temperature superposition behavior such as indicated in figure 8 applies, the two shift factors corresponding to the two temperatures T_1 and T_2 being $\phi_1 = \phi(T_1)$ and $\phi_2 = \phi(T_2)$. The analysis follows identical lines of reasoning as before, except that t is replaced by the appropriate t/ϕ. Thus equations (13) and (17) become, respectively

$$\alpha_{l1}(t) = C_1 e^{-(\mu/\phi_1)t} + C_2 \tag{31}$$

and

$$\alpha_{ul1}(t) = p_0[(C_2 + \beta)\frac{r_1}{r_\infty}(e^{r_\infty \lambda t_0} - 1) + \frac{C_1 r_1 \lambda}{\mu - r_\infty \lambda}(1 - e^{(r_\infty \lambda - \mu)t_0})]e^{-(r_\infty \lambda/\phi_2)t}. \tag{32}$$

We address first the question of stable/unstable deflection growth in the presence of these temperature variations. Following the same reasoning as that which led to equations (27) and (28) one finds that (27) is replaced by

$$\Delta\alpha_{\text{cycle}} = [e^{-(r_\infty \lambda/\phi_2 + \mu/\phi_1)t_0} - 1]\alpha(nt_0^-) + \alpha(0^+)(1 - e^{-r_\infty \lambda t_0/\phi_2})e^{-\mu t_0/\phi_1} + C_2(1 - e^{-\mu t_0/\phi_1}) \tag{33}$$

from which (28) becomes

$$p^*_{cr}(T) = \frac{r_\infty(1 + \frac{\phi_2}{\phi_1})}{\frac{\phi_2}{\phi_1} + r_\infty} \tag{34}$$

For constant temperature, equation (28) is recovered. We note that for the thermal variations considered here typically $\phi_1/\phi_2 \geq 1$ (and $r_\infty << 1$); as a consequence one has, with p_{cr} given by (28), that $p_{cr}/p^*_{cr} \leq 1$, with the implication that a load level which renders stable long-term deformations can lead to unstable growth in the presence of thermal cycling. An example of this situation is demonstrated in figure 9; here, the load level for the isothermal case illustrated in figure 5 for the example of stable deformation growth now causes unstable growth as the temperature excursions are added. It is important to recognize, however, that it is the cyclic nature of the temperature variations that is responsible for this unstable behavior and not merely a uniform change of the temperature: In the latter case, one would merely effect an acceleration of the time scale by which the deformation is achieved. The unstable behavior in the case of the cyclic temperature variation

results from the fact that during the loading portion of the cycle when the temperature is higher, deformations grow to a larger extent than they recover during the unloaded portion when the temperature is low and when the creep response is retarded.

3.1.4 Long-term stability conditions under various load and thermal behavior

As T_1/T_2 increases, ϕ_1/ϕ_2 decreases and, upon examining (34), we find that p^*_{cr} approaches r_∞. This can be interpreted as the deflection increasing rapidly during the high-temperature loaded portions of the cycle but recovering little during the lower-temperature unloading segments. If the recovery becomes negligible, the case of no recovery is approached (i.e. time-invariant loading), so that stability is determined by the generally very low rubbery buckling load corresponding to r_∞. On the other hand, as T_1/T_2 *decreases*, p^*_{cr} approaches unity: The retarded deflection during low-temperature loadings is recovered at an accelerated rate during unloading such that deformation does not accumulate, and only a load equal to the glassy buckling load, i.e., $p = 1$, can cause unstable deflection.

We include here also the results for the case where the loading and unloading portions of a cycle are of different durations t_1 and t_2

$$p^{**}_{cr}(T) = \frac{r_\infty(1 + \frac{t_1}{t_2}\frac{\phi_2}{\phi_1})}{\frac{t_1}{t_2}\frac{\phi_2}{\phi_1} + r_\infty}. \tag{35}$$

For constant temperature ($\phi_1 = \phi_2$) and equal loading and unloading durations ($t_1 = t_2$), equation (28) is recovered. Similar to equation (34), limits as t_1/t_2 approach infinity or zero give values of p^{**}_{cr} equal to r_∞ and unity, respectively, which is interpreted as representing cases of non-recovering, continuous loading and periodic impulsive loadings (under exclusion of material inertia).

3.2 Realistic material response illustrated by PMMA

Having dealt with the standard linear solid, primarily to establish the long-term stability boundary for the thermal cycling situation we turn to consideration of the counterpart problem but for a material with a realistically wide spectral distribution of relaxation times. As in Minahen & Knauss (1992) we employ the relaxation characteristics of polymethylmethacrylate (PMMA) as an exemplary material, though newer high-temperature materials will certainly possess more appropriate capabilities. However, we employ the properties of PMMA because these properties, including the time-temperature trade-off in the glassy and near-glassy domains, are well known; the same cannot be said about most or all of the polymers typically used in the manufacture of composite materials. Although PMMA is an uncrosslinked polymer and as such does not offer a long-term equilibrium modulus, we associate such a limit with the entanglement plateau. It is not the purpose of

this section to simply duplicate the earlier analysis for a different material, but to examine whether representations can be extracted from such an exercise that provides guidance for understanding qualitatively, and on a more realistic time-scale, the effect which cyclic loading can have on a thermoviscoelastic structure under constant and synchronous cyclical heating. In particular, we shall be interested in examining how the cyclic problem can be compared to that employing constant load as a reference, since the latter is readily computed approximately for realistic material behavior.

We use the relaxation modulus shown in figure 10 which represents the combined measurements by Lu (1992) and McLoughlin and Tobolsky (1952) except that we eliminate the very long-term flow regime and replace it by "rubbery" equilibrium behavior. [3] We recognize that this relaxation behavior is not precisely that of thermoplastic-matrix composites applications but we believe it to be representative if we do not limit ourselves to fiber-dominated lay-up configurations: in any case, this statement appears to us reasonable because we shall present all data and interpretations normalized by the short-time or glassy modulus. The governing integral equation (3) is evaluated numerically.

While we shall thus substitute for the relaxation or creep characteristics of a composite solid that of PMMA, with modifications as discussed above, it is imprudent to assess the behavior of carbon-reinforced polymers using the thermal expansion characteristics of PMMA. The reason is that the coefficient of thermal expansion of PMMA is about two orders of magnitudes larger than that of typical fiber-reinforced materials in the fiber direction, though, transverse to the latter, the expansion may also be large by comparison [see e.g., Schapery (1991)]. In order to deduce engineering-relevant information from these computations it is therefore reasonable to choose an appropriately small coefficient of axial thermal expansion and use, therefore, the "text value" of $\alpha_x = 3 \times 10^{-6}/°C$ [Tsai and Hahn].

A remark is in order on the criterion used to establish failure by buckling. Following Minahen and Knauss (1992), we use the attainment of a chosen deflection as the failure criterion. The time to failure is then the time to reach this deflection under any loading conditions. For demonstrative purposes, we may think of such a value as two or three multiples of the column thickness; we use a factor of 2.4 in this presentation.

Before turning to a comparison of the effect of a thermal gradient on the time scale of failure, we illustrate first four cases of column deflection history under cyclic loading for "realistic" material properties, namely subcritical, critical, and supercritical behavior, as well as a case for how the subcritical case can become supercritical (unstable) if thermal cycling accompanies loading. These situations are illustrated in figure 11 where the

[3] For computational purposes we represent the relaxation function by a series of exponentials (Prony-Dirichlet series) of 30 terms.

shaded area between each two curves represents the range of deformations as the column midpoint displacement increases under cyclic loading. The fourth figure in this group applies to the case of a load which, in the constant temperature case, is subcritical but which becomes supercritical when the temperature accompanying the load cycle increases load-synchronously by 10°C, similar to figure 9 for the standard linear solid. We note first that for material behavior with a large range of relaxation times it is no longer reasonably possible to computationally establish whether the deflection tends toward a limit value for very long (infinite) times. At best one observes that for supercritical loading the rate of growth increases with time, while for the critical and subcritical loading the converse seems to hold. This behavior follows from the previously developed long-term stability boundaries which are also valid for a material with realistic relaxation behavior.

It is apparent that under isothermal conditions any cyclic loading with maximal load amplitude p_0 will lead to failure after longer times than for the case when the same load p_0 acts invariantly with time; in fact, the same load which leads to eventual failure when constant may result in a long-term stable deflection when applied cyclically. On the other hand, it is of interest to examine the relative behavior between the two cases when the load in each case is normalized by its respective long-term stability boundary in such a way that the respective loads are related by

$$\left[\frac{p_0}{p_{cr}}\right]_{const} = \left[\frac{p_0}{p^*_{cr}}\right]_{cyc}, \tag{36}$$

because this comparison relates synchronous thermal and cyclic loadings to isothermal, time-invariant loads, the latter being readily estimable. As shown in figures 12–14, a very close agreement between the two responses is apparent. This result indicates that, while the realistic material response to cyclic loading may be analytically difficult and computationally time-consuming, the more-easily computed constant-load case can be used, by employing the above equivalence relation, to evaluate long-term behavior. It is worth noting that this equivalence *cannot* be used in comparing time-invariant and cyclic behavior in the case of the standard linear solid. Figures 15–17 clearly reveal this lack of correspondence. Although in the critical loading case the constant-load deflection follows the average deflection under cyclic load, the other two cases show divergence. The lack of a realistic range of relaxation times does not allow the above-determined equivalence to be applied for the simple material model [Schapery (1962)].

4. Effect of a Thermal Gradient

We next consider a column loaded axially at the center-line by a *step* load of magnitude P but in the presence of a transverse thermal gradient. Along the length of the column the temperature distribution is invariant. For these considerations we do not include an intrinsic initial imperfection, because the thermal gradient induces a lateral, stress-free deflection, which we designate by $w_0(x)$. Consider the coefficient of thermal expansion α to be a constant in the temperature range of interest.

Because of the thermoviscoelastic material behavior and the thermal gradient the effective properties vary across the thickness so that the neutral axis, located a distance $n(t)$ from the center-line, moves with time as dictated by (7) and is determined (numerically) by

$$n(t) = \frac{\int_{-\frac{h}{2}}^{\frac{h}{2}} z \int_{-\infty}^{t} E[t'(t,z) - \xi'(\xi,z)] \frac{\partial}{\partial \xi} \left[\frac{\partial u_0}{\partial x}(\xi) \right] d\xi \, dz}{\frac{P}{g} + \int_{-\frac{h}{2}}^{\frac{h}{2}} \int_{-\infty}^{t} E[t'(t,z) - \xi'(\xi,z)] \frac{\partial}{\partial \xi} \left[\frac{\partial u_0}{\partial x}(\xi) \right] d\xi \, dz} \tag{37}$$

However, it is first necessary to find $\partial u_0 / \partial x$.

Considering the purely axial compression of the column, force equilibrium requires

$$\int_A \sigma_x(z,t) \, dA = P \tag{38}$$

or

$$\int_{-\frac{h}{2}}^{\frac{h}{2}} \int_{-\infty}^{t} E[t'(t,z) - \xi'(\xi,z)] \frac{\partial}{\partial \xi} \left[\frac{\partial u_0}{\partial x}(\xi) \right] d\xi \, dz = P. \tag{39}$$

Discretization of this equation allows determination of $\partial u_0 / \partial x$ by iteration and via the Newton-Raphson method. Once $\partial u_0 / \partial x$ is known, one solves (37) for $n(t)$. Finally, knowing $n(t)$, one solves (8) for the displacement $A(t)$ by discretization and the Newton-Raphson method.

For the case of a transversely linear temperature gradient,

$$T(z) = az + b \tag{40}$$

and employing the Prony-Dirichlet series representation

$$E(t) = E_\infty + \sum_{k=1}^{s} E_k e^{-\lambda_k t} \tag{41}$$

along with the time-temperature superposition factor $a(T)$, the relaxation modulus becomes, for any value of z,

$$E(z,t) = E_\infty + \sum_{k=1}^{s} E_k e^{-\frac{\lambda_k}{a[T(z)]} t} \tag{42}$$

or

$$E(z,t) = \sum_{k=0}^{s} E_k e^{-\frac{\lambda_k}{a[T(z)]} t} \tag{43}$$

where E_∞ is the 0^{th}-order coefficient. At $t = 0^+$, we define

$$E_g \equiv E(z, 0^+) = E_\infty + \sum_{k=1}^{s} E_k. \tag{44}$$

4.1 Analytical preliminaries

The thermal gradient introduces an initial curvature which can be computed as for an elastic solid if one assumes that the coefficients of thermal expansion are time-insensitive. The analysis follows essentially that outlined in Timoshenko and Goodier (1987) and details are also presented in [Tsuyuki and Knauss (1992)]. The result of that analysis is, with coordinate definition as given in figure 18,

$$w_0(x) = -\frac{1}{2}\alpha_x a \left[\left(x - \frac{l}{2}\right)^2 - \frac{l^2}{4}\right] \tag{45}$$

Express w_0 in a Fourier series

$$w_0(x) = \sum_{m=1}^{\infty} B_m \sin\frac{m\pi x}{l} \tag{46}$$

so that

$$B_m = -\frac{2}{l}\int_0^l \frac{1}{2}\alpha_x a \left[\left(x - \frac{l}{2}\right)^2 - \frac{l^2}{4}\right] \sin\frac{m\pi x}{l}\, dx \tag{47}$$

$$B_m = \begin{cases} \frac{4\alpha_x a l^2}{(m\pi)^3} & \text{if m odd;} \\ 0 & \text{if m even .} \end{cases} \tag{48}$$

And thus

$$B_1 = \frac{4\alpha_x a l^2}{\pi^3} \tag{49}$$

or, more generally,

$$B_m = \frac{B_1}{m^3} \tag{50}$$

Thus a one-term approximation with B_1 alone is not unreasonable for present purposes. In fact, in view of [Sechler] this choice would render the estimates of instability occurrence conservative.

In conformity with the step loading one finds [from (39)] that, immediately after load application ($t = 0^+$),

$$\int_{-\frac{h}{2}}^{\frac{h}{2}} E_g \frac{\partial u_0}{\partial x}(0^+)\, dz = P \tag{51}$$

or

$$\epsilon_0 \equiv \frac{\partial u_0}{\partial x}(0^+) = \frac{1}{E_g}\frac{P}{h} \tag{52}$$

and similarly for (7) and (8) that

$$n_0 \equiv n(0^+) = 0 \tag{53}$$

and

$$A(0^+) = \frac{B}{\frac{E_g I}{P}\left(\frac{\pi}{l}\right)^2 - 1}. \tag{54}$$

For the case that the column reaches a stable equilibrium at large times, one determines the long-term result by observing that $E(z,t) \to E_\infty$ as $t \to \infty$. Then (39) becomes

$$E_\infty \int_{-\frac{h}{2}}^{\frac{h}{2}} \int_{-\infty}^{t} \frac{\partial}{\partial \xi}\left\{\frac{\partial u_0}{\partial x}(\xi)\right\} d\xi\, dz = P \tag{55}$$

or

$$\epsilon_\infty \equiv \left.\frac{\partial u_0}{\partial x}\right|_\infty = \frac{1}{E_\infty}\frac{P}{h}. \tag{56}$$

Similarly, (37) leads to

$$n_\infty \equiv n(\infty) = 0 \tag{57}$$

and finally, (8) gives the complement to (54) as

$$A(\infty) = \frac{B}{\frac{E_\infty I}{P}\left(\frac{\pi}{l}\right)^2 - 1}. \tag{58}$$

We next evaluate the stability regimes of the column, following Minahen and Knauss (1992). We rewrite (56) and (58) as

$$A(0^+) = \frac{PB}{P_{cr}^0 - P} \quad : \qquad P_{cr}^0 \equiv E_g I\left(\frac{\pi}{l}\right)^2 \tag{59}$$

and

$$A(\infty) = \frac{PB}{P_{cr}^\infty - P} \quad : \qquad P_{cr}^\infty \equiv E_\infty I\left(\frac{\pi}{l}\right)^2. \tag{60}$$

P_{cr}^0 and P_{cr}^∞ are the Euler buckling loads based on the instantaneous (glassy) and long-term (rubbery) moduli, respectively, and if P approaches these values, the glassy and long-term responses, respectively, become unbounded. This establishes three stability regimes. If the load is less than P_{cr}^∞ (60), the deflection eventually tends to the value given by (58). If the load exceeds P_{cr}^0 (59), the column buckles instantaneously. If the load level falls between

these limits, the deflection grows gradually in an unbounded manner. This is illustrated in figure 18, where the column response of a load at 1% *below* P_{cr}^{∞} is illustrated; the "supercritical" load is one percent *above* that critical load.

4.2 Time-dependent failure—design life

Once the column has (we assume instantly) attained the initial imperfection given by equations 46 and 48, the subsequent column behavior is a direct response to the axial load; however, in contrast to the case of uniform temperature, different layers of the material through the thickness creep/relax at different rates in dependence on the local temperature. In view of the previous experience with buckling solutions involving viscoelastic material behavior there is little expectation that this problem can be solved in "closed form" and we therefore address the solution numerically.

Before delineating that development we comment on the definition of "failure" in the present context. As observed in Minahen and Knauss (1992), the failure of a viscoelastic column approaches instability over potentially very long time scales. While any load level above that corresponding to the relaxation modulus will result in loss of stability at infinite time, it may require potentially very long times to attain deflections that are unacceptable from an engineering point of view. We thus define a "design-life" which is that time required for the column to achieve a prescribed "critical" displacement. As in previous work we arbitrarily choose this deflection as about 2.5 times the column thickness. [4] With this concept in mind we model a column 500 mm in length and 6.35 mm thick having the thermoviscoelastic properties of PMMA as discussed above, but the thermal expansion characteristics of a carbon-epoxy composite $\alpha = 3 \times 10^{-6}/°C$ as reported in [Tsai and Hahn].

The evaluation of equations (8), (37), and (39) is accomplished numerically under the assumption that a one-term expansion of (5) with (6.46) is sufficient for our purposes. An outline of the numerical procedure is summarized in the Appendix.

For reference purposes it is prudent to record the lifetimes at a constant temperature of 100°C as shown in figure 10 [Minahen and Knauss (1992)]: As demonstrated in that reference, the relaxation modulus provides a good engineering estimate for this relation if proper account is taken of a horizontal shift along the log-time axis of approximately one decade, which is, however, a function of the initial column imperfection.

Because in applications of high-speed transports one surface of the structure is likely to be

[4] It has been shown in Minahen and Knauss (1992) that for this deflection magnitude the current linearized formulation is adequate and that the kinematically non-linear formulation is not required. The value 2.5 is, in reality, a value of 2.4 in the earlier work which incorporated factors arising out of a dimensional conversion in connection with the experimental work reported there.

maintained at a constant temperature, we consider here also the case when one side of the column is kept at 30°C; the other side is exposed to a temperature varying between this value and 120°C, so that one surface experiences the extreme conditions of being above the glass transition temperature. The results are delineated in figure 20. It is clear that with increasing thermal gradient across the column its life decreases rapidly; this is the result of both the increase in the bowing induced by the thermal gradient ("initial imperfection") and the thermoviscoelastic acceleration associated with the increased temperature. However, while uniformly increasing temperatures allow a time-temperature trade-off in the form of a simple shifting of the failure curves along the logarithmic time axis, that is no longer even approximately the case. In fact, it is difficult to make the case that the isothermal response provides a generally conservative estimate of the failure times.

Observing the effect of heating one side of the column to above the glass transition temperature while keeping the other one at 30°C we see that the life of the column has been decreased by about five orders of magnitude relative to the isothermal 30°C case. This result is readily understood if one recognizes that in addition to the large time-accelerating effect of high temperatures below the glass transition the stiffness of the polymer has virtually disappeared for temperatures above 110°C so that the column has effectively "lost thickness."

5. Conclusion

The evolution of unstable lateral deformations in a thermoviscoelastic column has been investigated under the conditions of cyclic loading with synchronous temperature excursions, as well as time-invariant loading while subject to a transverse temperature gradient. Stability analysis in the cyclic loading case indicates that, while such loading under isothermal conditions leads to stable long-term deflections at loads greater than the rubbery buckling load (and therefore the long-term stability limit for constant loading), the addition of temperature cycling can induce unstable long-term deflection in cases with otherwise subcritical load levels, even with relatively small temperature changes. Evaluation of the behavior of a material with a realistic time-response spectrum as represented by that of PMMA leads to the conclusion that the envelope of deflections of a realistic material under cyclic loading can be approximated by the response to constant loading when an appropriate equivalent load normalization is used.

While it appears difficult to recognize a general scaling process for the time-dependent response under various thermal gradients, it is possible to give some general guidelines or rough estimates for bounding failure response. To see this, we plot in figure 21 the responses for the different gradients from figure 20, but time-shifted by the average temperature across the column. The solid curve in that figure represents the failure time for the column at the uniform reference temperature (30°C, and in shape equal to the relaxation modulus of figure 10). Thus, if the gradients were small, all curves would (nearly) collapse into the single (solid) curve. One notes clearly that for loads above 90% of the "glassy buckling

load," all failures at elevated temperatures occur sooner by several orders of magnitude than at a reference state corresponding to the average temperature. Thus, the use of an average temperature for estimating the time response in the presence of temperature gradients provides a massivly non-conservative failure time. [5] On the other hand, it is also clear that assuming the failure behavior for a structure exposed to the maximum temperature provides an extremely conservative estimate of its failure response, but one that may be useful for initial design estimation.

This study has been conducted on a macroscopic level, but a last word concerning comparison to the local fiber buckling case is in order. Indeed the results should be applicable in some sense to localized phenomena, for, while the boundary conditions differ, the essential aspects of the time-dependence and subsequent response do not. It should be noted that the "initial imperfection" used in the gradient problem is entirely due to the thermoelastic expansion of the material, and, assuming a positive coefficient, this will always result in the outside of the "bowing" being the hot side of the column, and the hot (accelerated time-response) side therefore tending to be in tension. However, if a specific case arises where the heating is coupled with some transverse loading such that this tendency is overcome and the bowing reverses, ending up with the hot side in compression, the local fiber buckling/crimping becomes a much more critical issue, due to the decreasing local stiffness. In the majority of cases likely to be encountered in real-life application, however, the "hot-side-out" assumption is adequate.

Acknowledgments: The authors would like to acknowledge the support of the National Aeronautics and Space Administration through grant number NSG 1483 with Dr. James Starnes as the technical officer.

[5] The fact that this trend appears to reverse below 90% is not really correct since these curves have all been shifted along the time axis in accordance with the time-temperature reduction according to the average temperature.

References

Arnold, S.M., (1987) "Effects of State Recovery on Creep Buckling Induced by Thermomechanical Loading," Ph.D. Thesis, University of Akron. Akron, Ohio

Bodner, S.R., (1991) "A Lower Bound on Bifurcation Buckling of Viscoplastic Structures," ASME Winter Annual Meeting.

Distefano, J.N., (1965) "Creep Buckling of Slender Columns," *Journal of the Structural Division, ASCE*, 91, No. 3, p. 127.

Drozdov, A., (1991) Personal Communications and (1) "Stability of Rods of Nonuniform-Aging Viscoelastic Material." *Mechanics of Solids*. 1984, 2. pp. 176-186, (co-authors: V.B. Kolmanovskii, V.D. Potapov). (2) "Stability of Beams Made of a Non-Homogeneous, Aging, Viscoelastic Material." *Dokl. Akad. Nauk Arm SSR*, 1984, 78(3), pp. 117–121, (co-authors: V.B. Kolmanovskii, V.D. Potapov). [in Russian]

Glockner, P.G. and Szyszkowski, W., (1987) "On the Stability of Columns Made of Time Dependent Materials." in *Civil Engineering Practice* Vol. 1, (Structures) Chapter 23, ed. P.N. Cheremisinoff, N.P. Cheremisinoff and S.L. Cheng.

Hilton, H.H., (1952) "Creep Collapse of Viscoelastic Columns with Initial Curvatures," *Journal of the Aeronautical Sciences*, 19, p. 844.

Hoff, N.J., (1956) "Creep Buckling." *Aeronautical Quarterly*, 7, p. 1.

Huang, N.C., (1976) "Creep Buckling of Imperfect Columns." *Journal of Applied Mechanics* E43, No. 1, p. 131.

Kempner, J., (1962) "Viscoelastic Buckling." in *Handbook of Engineering Mechanics* ed. F. Flügge, McGraw-Hill Book Company

Lu, H., (1992) Personal Communications. California Institute of Technology

McLoughlin, J.R. and Tobolsky, A.V., (1952) "The Elastic Behavior of Polymethylmethacry-

late," *Journal of Colloid Science* **7** p. 555

Minahen, T.M. and Knauss, W.G., (1993) "Creep Buckling of Viscoelastic Structures," *International Journal of Solids and Structures*. Vol. 30. No. 8, pp. 1075–1092.

Salchev, L.Z. and Williams, J.G., (1969) "Bending and Buckling Phenomena in Thermoplastic Beams," *Plastics and Polymers*, 37, p. 159.

Schapery, R.A. (1962). "Approximate Methods of Transform Inversion for Viscoelastic Stress Analysis" in *Proceedings of the 4th U.S. National Congress of Applied Mechanics* pp. 1075–1085. New York, NY

Schapery, R.A., (1991). "Analysis of Local Buckling in Viscoelastic Composites," presentation at the *IUTAM Symposium on Local Mechanics Concepts for Composite Material Systems* VPI and State University

Sechler, E.E., (1952) *Elasticity in Engineering*. John Wiley and Sons, New York, NY

Timoshenko, S.P. and Goodier, J.N., (1987) *Theory of Elasticity*. McGraw Hill Book Company, New York, NY

Tsai, S.W. and Hahn, H.T., (1980) *Introduction to Composite Materials*. Technomic Publishing Company, Westport, CT Tsuyuki, R.M. and Knauss, W.G., (1992) *Buckling of Thermoviscoelastic Structures Under Temporal and Spatial Temperature Variations*. California Institute of Technology, Graduate Aeronautical Laboratories, SM 92-46; December, 1992

Appendix: Numerical Procedure

The results in section 4.2 are obtained by solving equation (8) for $A(t)$. (8), however, contains $n(t)$, which is given by equation (37). (37) in turn contains $\partial u_0/\partial x$, which must be determined from equation (39). A sequence thus evolves for the determination of $A(t)$: for each time step, (39) is solved for $\partial u_0/\partial x$, which allows $n(t)$ to be determined from (37). (8) can then be solved for $A(t)$. This sequence is carried out in a computer program which, after initializing material constants (Prony terms and WLF constants) and geometric and loading parameters, executes a time loop. The time loop contains three sections which at each time step solve for $\partial u_0/\partial x$, $n(t)$, and $A(t)$, respectively.

While (37) requires only simple numerical integration, (8) and (39) are implicit equations which are solved using a Newton-Raphson approach. (Note that a similar routine is executed for section 3.2, except normalizations.) A special recursive relation is defined in order to facilitate time-stepping without having to preserve previous values of parameters for the convolution. The same methodology is used to solve both (8) and (39); here we only give the details for the solution of (8), trusting that the analogy for (39) will be apparent [note that the results of section 3.2 are obtained by an essentially identical procedure, except for the use of the normalizations given in (9)]. We recast (8) in Riemann form and define the function

$$
\begin{aligned}
F(t) = \left(\frac{\pi}{l}\right)^2 \int_{-\frac{h}{2}}^{\frac{h}{2}} [z - n(t)] \Bigg\{ & [z - n(0^+)] A(0^+) E(z,t) \\
& + \int_{0^+}^{t} E(z, t-\xi) \frac{\partial}{\partial \xi} \left\{ [z - n(\xi)] A(\xi) \right\} d\xi \Bigg\} dz \\
& - P\,[A(t) + B].
\end{aligned}
$$

which for $F(t) = 0$ solves (8). This function is discretized at a sequence of distinct times t_r and with respect to z as

$$
\begin{aligned}
F(t_r) \equiv & F_r \\
= & \left(\frac{\pi}{l}\right)^2 \sum_{i=1}^{q} [z_i - n(t_r)] \Bigg\{ z_i A(0^+) E(z_i, t_r) \\
& + \sum_{j=1}^{r} E(z_i, t_r - t_{j-1}) \frac{\Delta \left\{ [z_i - n(t_j)] A(t_j) \right\}}{\Delta t} \Delta t \Bigg\} \Delta z \\
& - P\,[A(t_r) + B].
\end{aligned}
$$

Using (15) for $E(z,t)$, there follows

$$F_r = \left(\frac{\pi}{l}\right)^2 \sum_{i=1}^{q} [z_i - n(t_r)] \Bigg\{ z_i A(0^+) \sum_{k=0}^{s} E_k e^{-\frac{\lambda_k}{\phi(z_i)} t_r} + \sum_{j=1}^{r} \sum_{k=0}^{s} E_k e^{-\frac{\lambda_k}{\phi(z_i)}(t_r - t_{j-1})} \Delta\{[z_i - n(t_j)] A(t_j)\} \Bigg\} \Delta z - P\,[A(t_r) + B].$$

Define

$$G_r^{k,i} \equiv \sum_{j=1}^{r} E_k e^{-\frac{\lambda_k}{\phi(z_i)}(t_r - t_{j-1})} \Delta\{[z_i - n(t_j)] A(t_j)\}$$

so that

$$F_r = \left(\frac{\pi}{l}\right)^2 \sum_{i=1}^{q} [z_i - n(t_r)] \Bigg\{ z_i A(0^+) \sum_{k=0}^{s} E_k e^{-\frac{\lambda_k}{\phi(z_i)} t_r} + \sum_{k=0}^{s} G_r^{k,i} \Bigg\} \Delta z - P\,[A(t_r) + B].$$

Upon isolating the term for $j = r$ from the series for $G_r^{k,i}$ one finds

$$\begin{aligned} G_r^{k,i} =& E_k e^{-\frac{\lambda_k}{\phi(z_i)} \Delta t} \Delta\{[z_i - n(t_r)] A(t_r)\} \\ &+ \sum_{j=1}^{r-1} E_k e^{-\frac{\lambda_k}{\phi(z_i)}(t_r - t_{j-1})} \Delta\{[z_i - n(t_j)] A(t_j)\} \\ =& E_k e^{-\frac{\lambda_k}{\phi(z_i)} \Delta t} \Delta\{[z_i - n(t_r)] A(t_r)\} \\ &+ e^{-\frac{\lambda_k}{\phi(z_i)} \Delta t} \sum_{j=1}^{r-1} E_k e^{-\frac{\lambda_k}{\phi(z_i)}(t_{r-1} - t_{j-1})} \Delta\{[z_i - n(t_j)] A(t_j)\} \end{aligned}$$

and the sum is now equal to the previous value of $G_r^{k,i}$, i.e., $G_{r-1}^{k,i}$ so that we may write

$$\begin{aligned} G_r^{k,i} =& E_k e^{-\frac{\lambda_k}{\phi(z_i)} \Delta t} \Delta\{[z_i - n(t_r)] A(t_r)\} \\ &+ e^{-\frac{\lambda_k}{\phi(z_i)} \Delta t} G_{r-1}^{k,i}. \end{aligned}$$

This recursive relation allows solution of the equation at successive time steps without having to retain solutions for all prior times. We can also calculate

$$\frac{\partial F_r}{\partial A} = \left(\frac{\pi}{l}\right)^2 \sum_{i=1}^{q} [z_i - n(t_r)]^2 \sum_{k=0}^{s} E_k e^{-\frac{\lambda_k}{\phi(z_i)} \Delta t} \Delta z - P.$$

Then, using the Newton-Raphson method, where A' is the current estimate for A and A'' is the updated value,

$$A'' = A' + \Delta A$$

$$\begin{aligned} F_r(A'') &= F_r(A' + \Delta A) \\ &= F_r(A') + \frac{\partial F_r(A')}{\partial A}\Delta A + \cdots \end{aligned}$$

We wish to find $F_r = 0$, so

$$0 = F_r(A') + \frac{\partial F_r(A')}{\partial A}\Delta A + \cdots$$

Therefore we approximate:

$$\Delta A = -\frac{F_r(A')}{\partial F_r/\partial A}.$$

Figure Captions

Figure 1: Viscoelastic column under axial loading and reference frame definition.

Figure 2: Synchronous load and thermal history.

Figure 3: Response curve for growth of buckling deflection under constant load and isothermal conditions [see Minahen and Knauss].

Figure 4: Illustration of piece wise construction of response under cyclic "square" loading.

Figure 5: Response of column (standard linear solid) under isothermal, cyclic loading for $p < p_{cr}$

Figure 6: Response of column (standard linear solid) under isothermal, cyclic loading for $p = p_{cr}$

Figure 7: Response of column (standard linear solid) under isothermal, cyclic loading for $p > p_{cr}$

Figure 8: Time-temperature shift factor for PMMA, also used for exemplary standard linear solid.

Figure 9: Response of the standard linear solid for the same (stable) load level as in Figure 5, but now with a load-synchronous thermal excursion added.

Figure 10: Relaxation Modulus for PMMA. The shape of this curve is the same as that for the time to failure of an isothermal column under constant load [See Minahen and Knauss. The upper portion of this curve is also the same as the solid curves in figures 20 and 21].

Figure 11: Response characteristics of a column possessing PMMA properties under isothermal conditions and with load-synchronous heating.

Figure 12: Comparison of response under steady load (dashed line, $p=p_0(1+r_\infty)/2)$) and cyclical loading (solid curve, $p=r_\infty$) according to equation 36 for PMMA properties and $p < p_{cr}$

Figure 13: Comparison of response under steady load (dashed line, $p=p_0(1+r_\infty)/2)$) and cyclical loading (solid curve, $p=r_\infty$) according to equation 36 for PMMA properties and $p = p_{cr}$

Figure 14: Comparison of response under steady load (dashed line, $p=p_0(1+r_\infty)/2$) and cyclical loading (solid curve, $p=r_\infty$) according to equation 36 for PMMA properties and $p > p_{cr}$

Figure 15: Comparison of response under steady load (solid line) and cyclical loading (dashed curve) according to equation 36 for the standard linear solid and $p < p_{cr}$

Figure 16: Comparison of response under steady load (solid line) and cyclical loading (dashed curve) according to equation 36 for the standard linear solid and $p = p_{cr}$

Figure 17: Comparison of response under steady load (solid line) and cyclical loading (dashed curve) according to equation 36 for the standard linear solid and $p > p_{cr}$

Figure 18: Configuration of the column under a thermal gradient.

Figure 19: Example of critical loading. The solid and dashed curves represent responses of a standard linear solid to loads which are, respectively, 1% above and below the long term critical value.

Figure 20: Failure time (= design life) versus normalized column load P/E_g for various thermal gradients across the column. One surface of the column is held at 30^0C while the other is kept at a higher temperature by the amounts indicated. Note that the solid curve has the shape of the upper portion of the curve in Figure 10.

Figure 21: The responses of figure 20 plotted with the time axis adjusted by time-temperature superposition with respect to the average column temperature. In this plot small or zero gradients would make all curves coincide (approximately) with the solid curve.

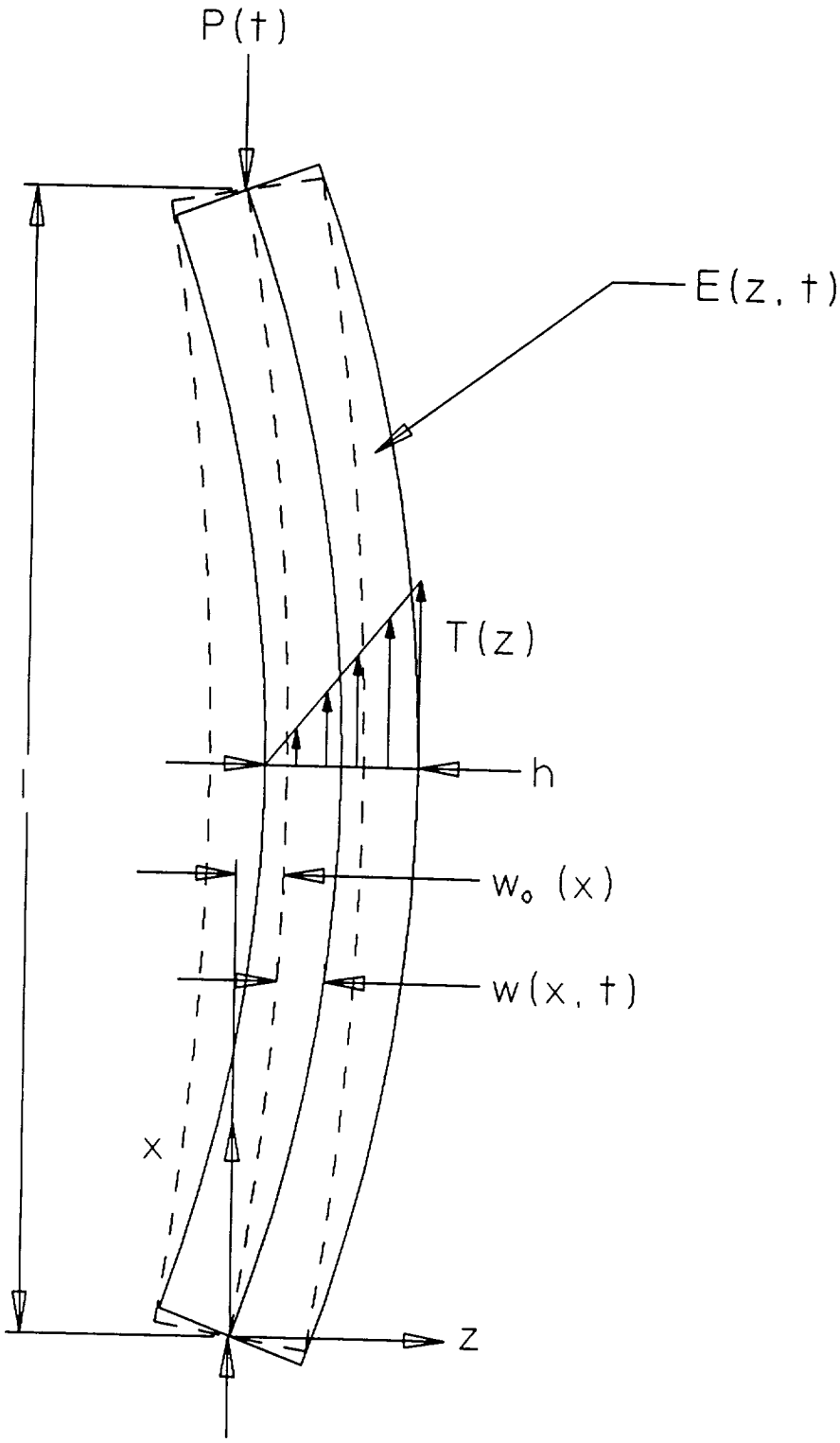

igure 1: Viscoelastic Column Under End Load

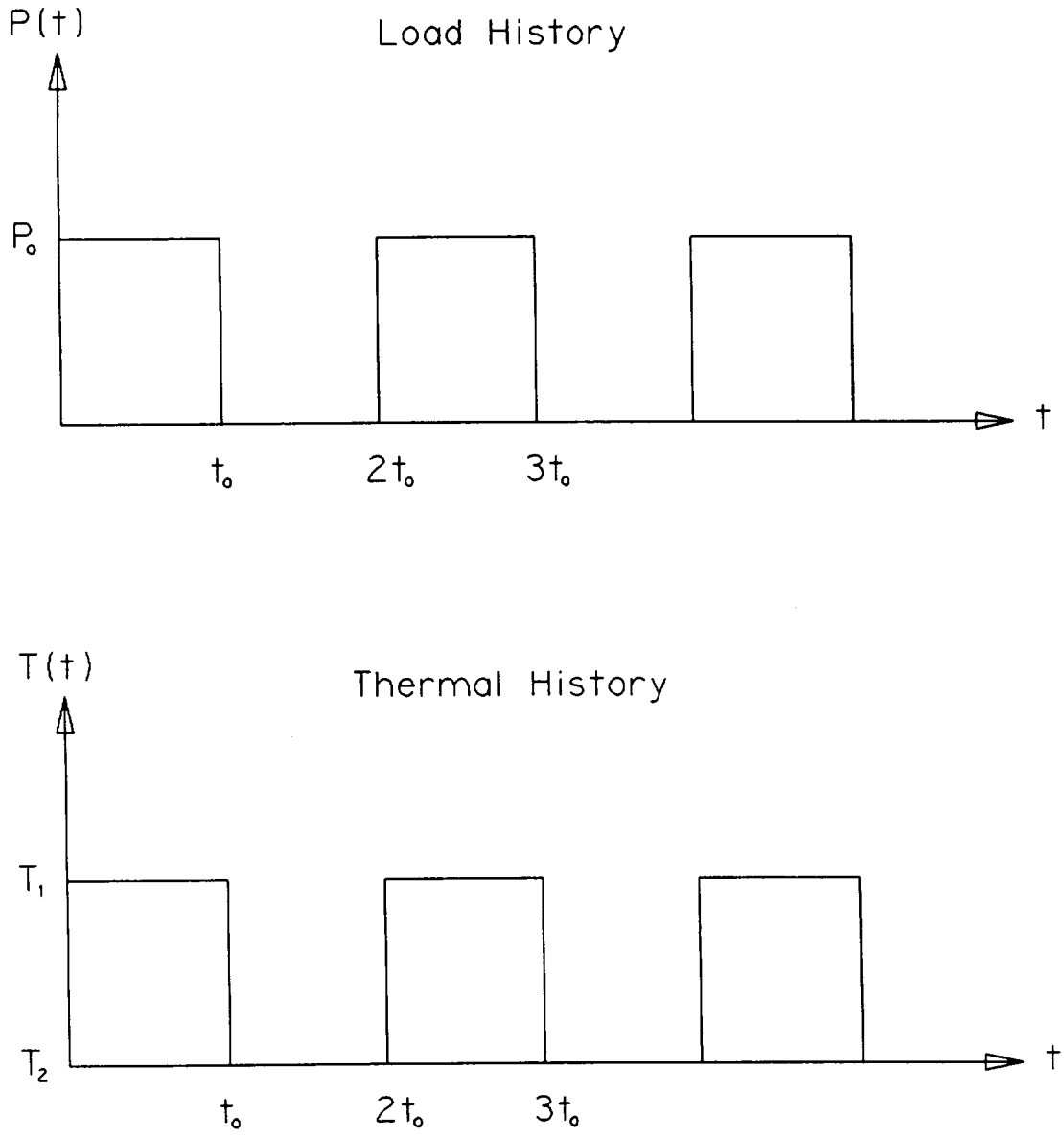

Figure 2: Cyclic Loading

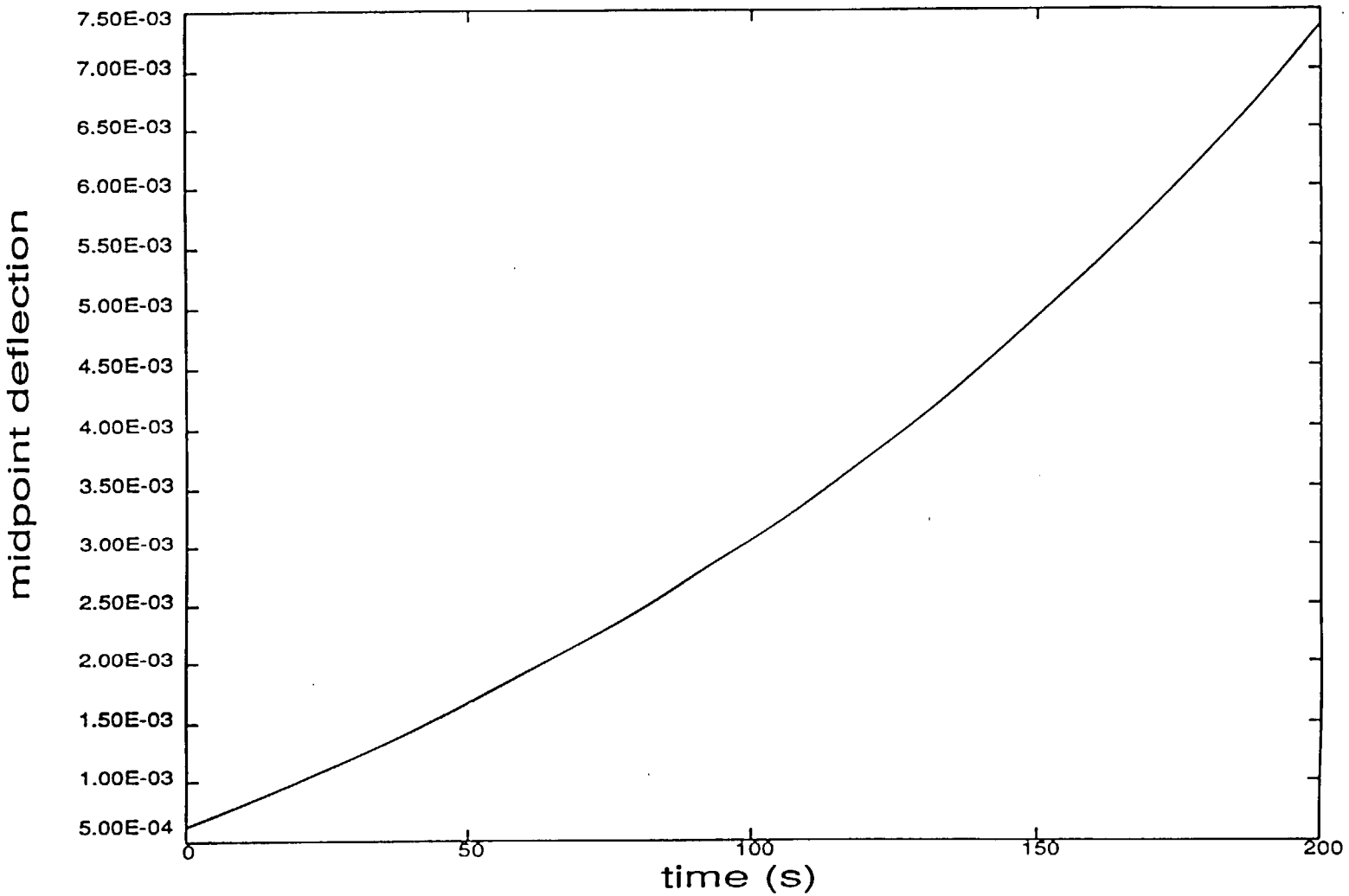
7.50E-03
7.00E-03
6.50E-03
6.00E-03
5.50E-03
5.00E-03
4.50E-03
4.00E-03
3.50E-03
3.00E-03
2.50E-03
2.00E-03
1.50E-03
1.00E-03
5.00E-04
midpoint deflection
0
50
100
150
200
time (s)

Figure 3

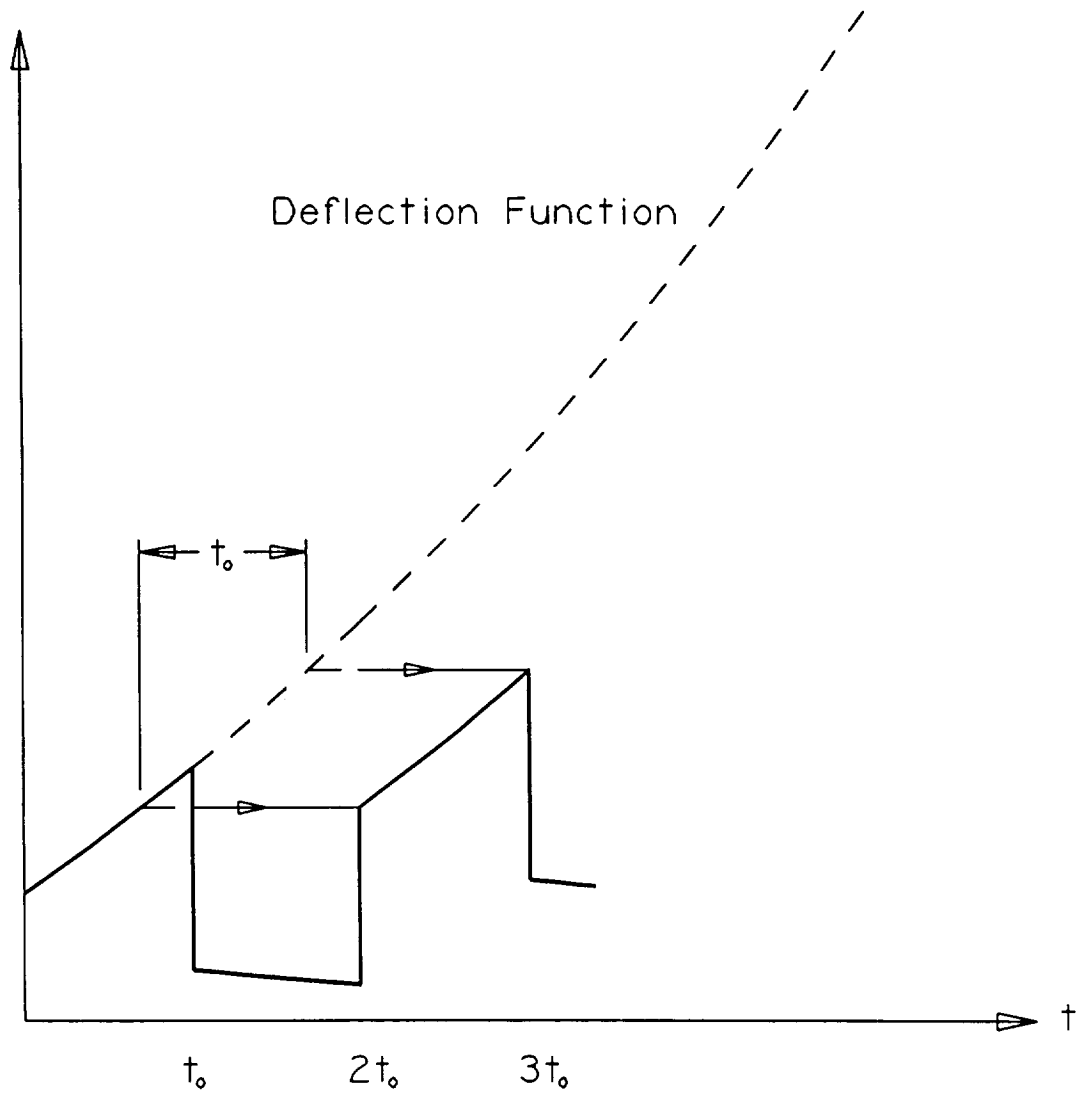

Figure 4: Illustration of the Piecewise Procedure

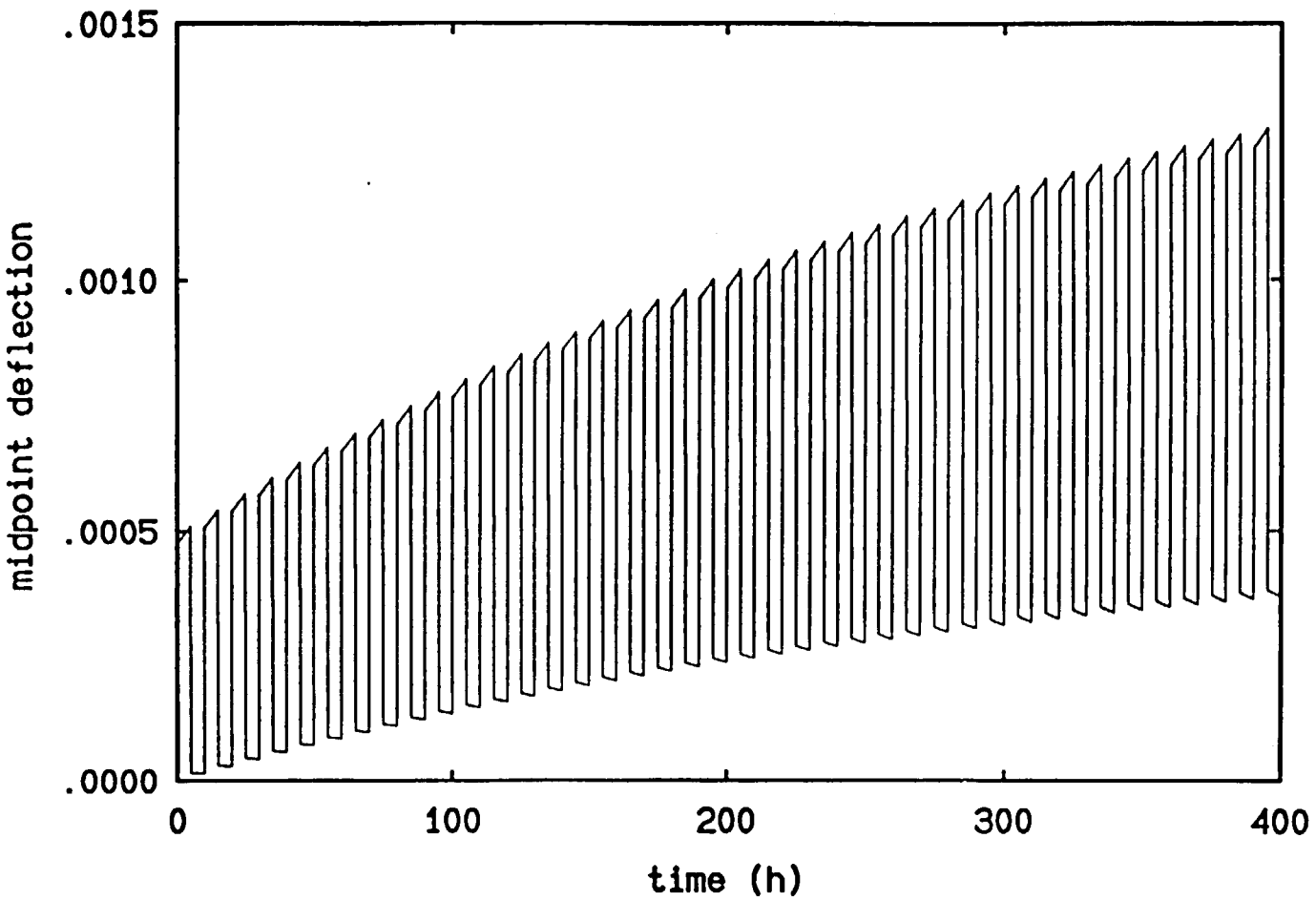
.0015
.0010
.0005
.0000
midpoint deflection
0
100
200
300
400
time (h)

Figure 5

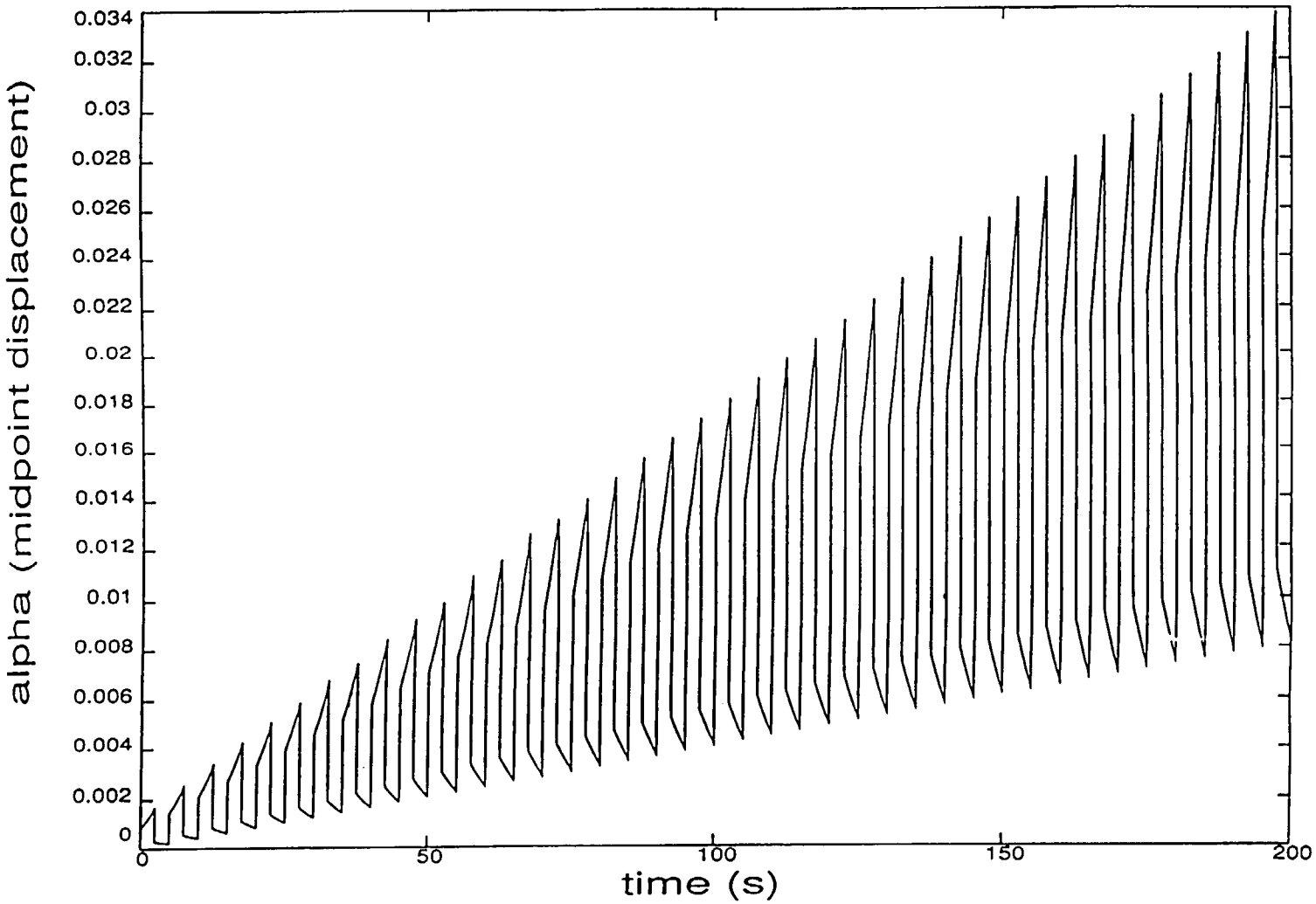
alpha (midpoint displacement)
0.034
0.032
0.03
0.028
0.026
0.024
0.022
0.02
0.018
0.016
0.014
0.012
0.01
0.008
0.006
0.004
0.002
0
0
50
100
150
200
time (s)

Figure 6

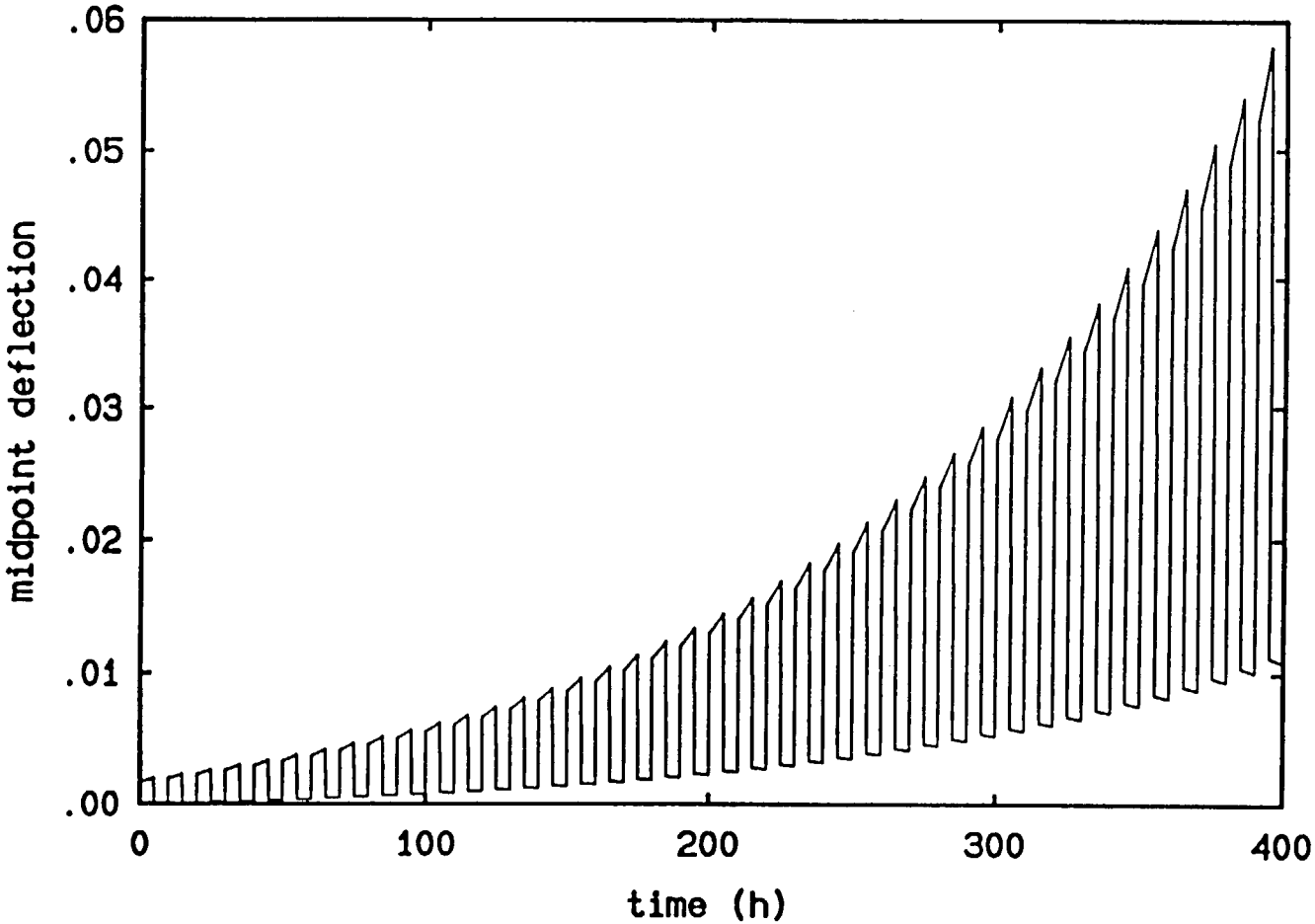
.06
.05
.04
.03
.02
.01
.00
midpoint deflection
0
100
200
300
400
time (h)

Figure 7

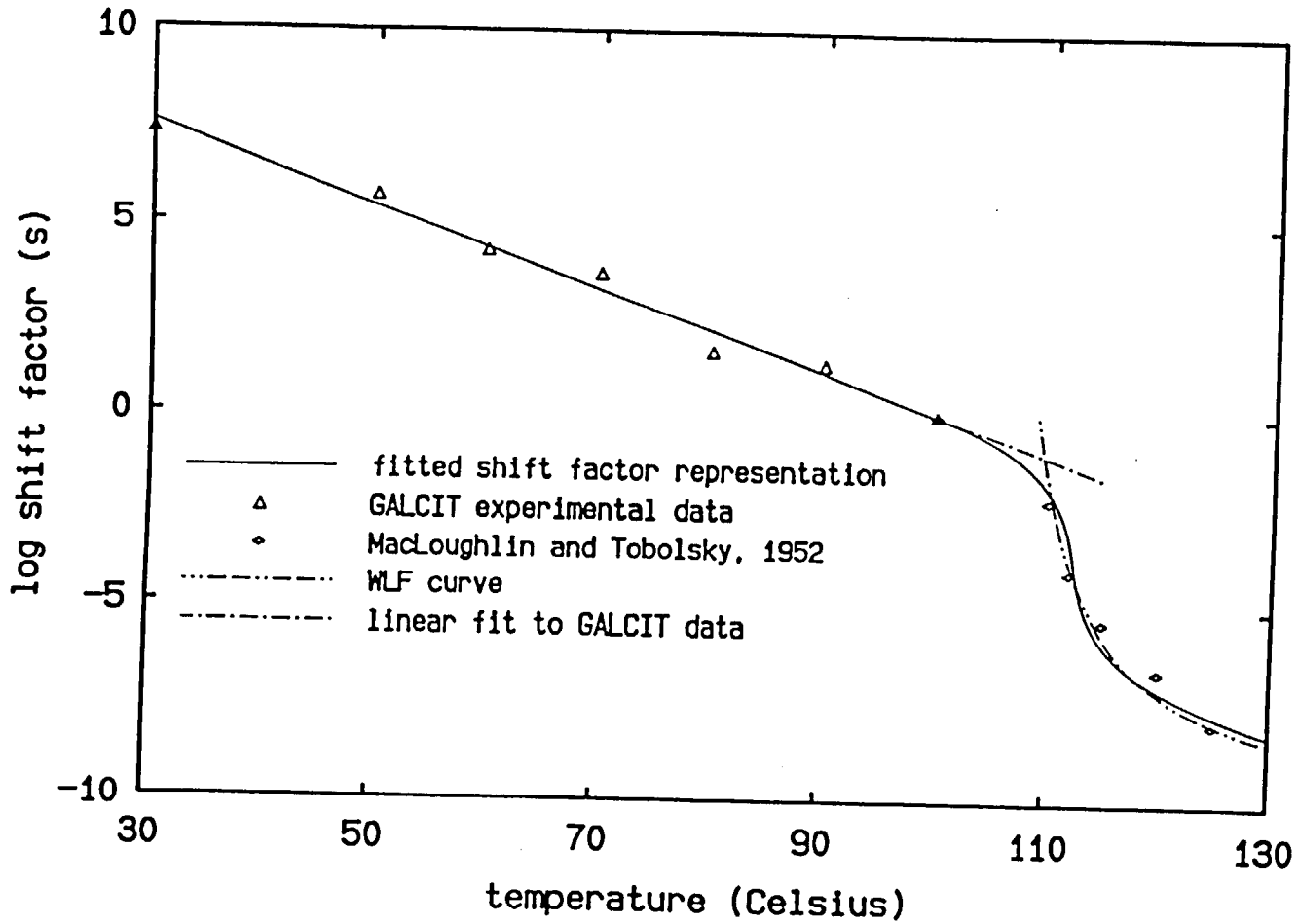
10
5
0
-5
-10
30
50
70
90
110
130
log shift factor (s)
temperature (Celsius)
fitted shift factor representation
GALCIT experimental data
MacLoughlin and Tobolsky, 1952
WLF curve
linear fit to GALCIT data

Figure 8

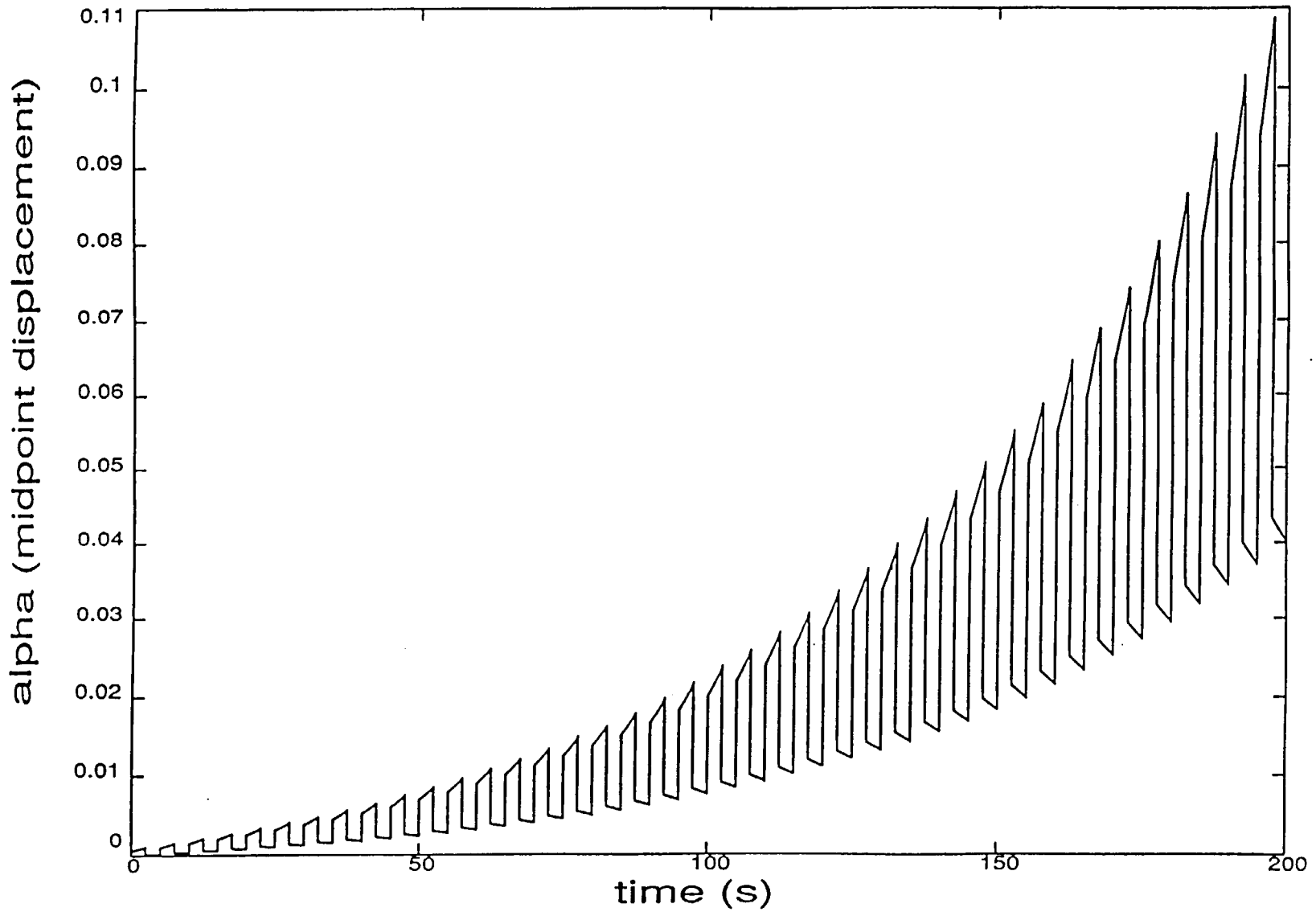
alpha (midpoint displacement)
0.11
0.1
0.09
0.08
0.07
0.06
0.05
0.04
0.03
0.02
0.01
0
0
50
100
150
200
time (s)

Figure 9

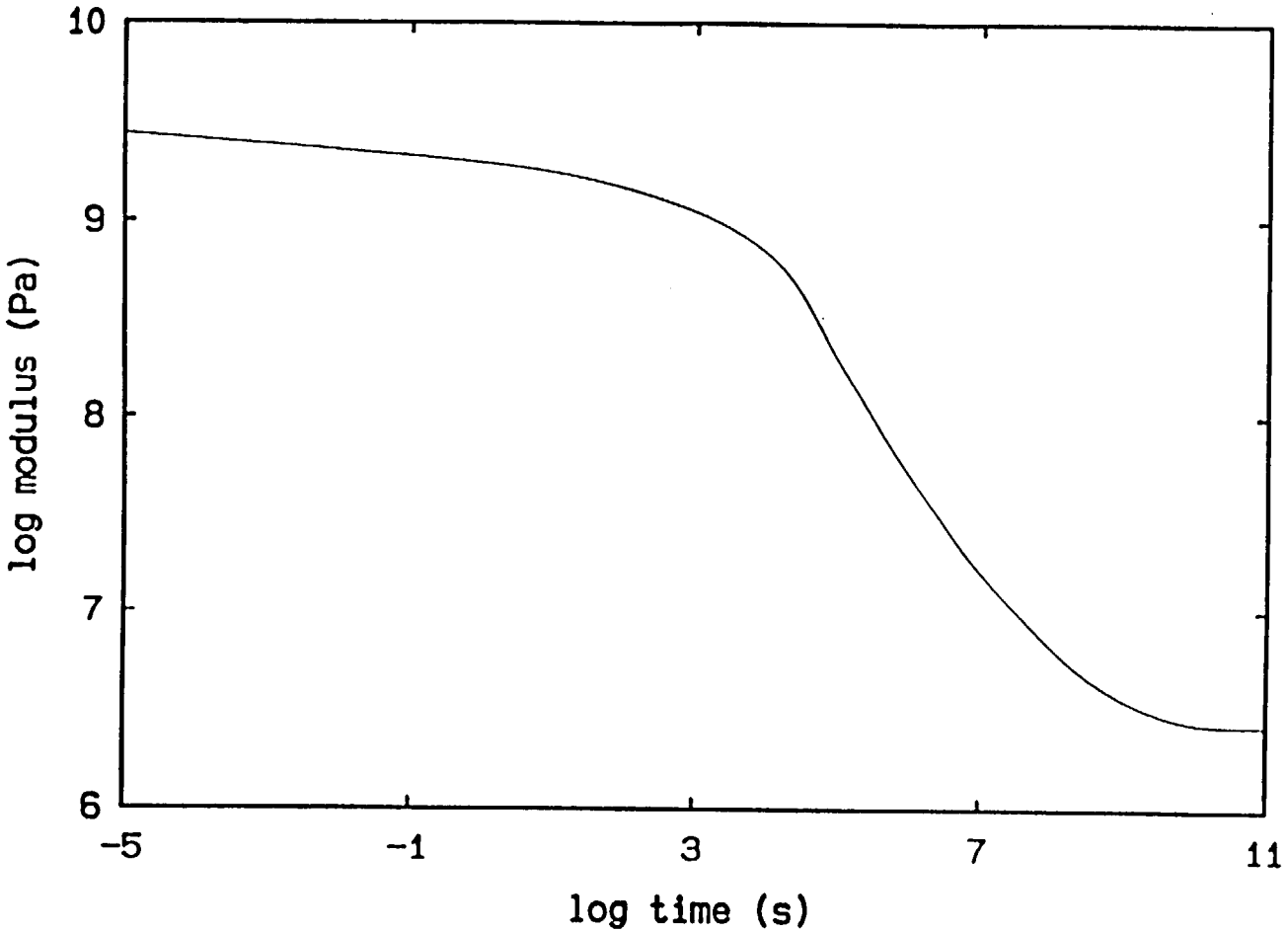

Figure 10

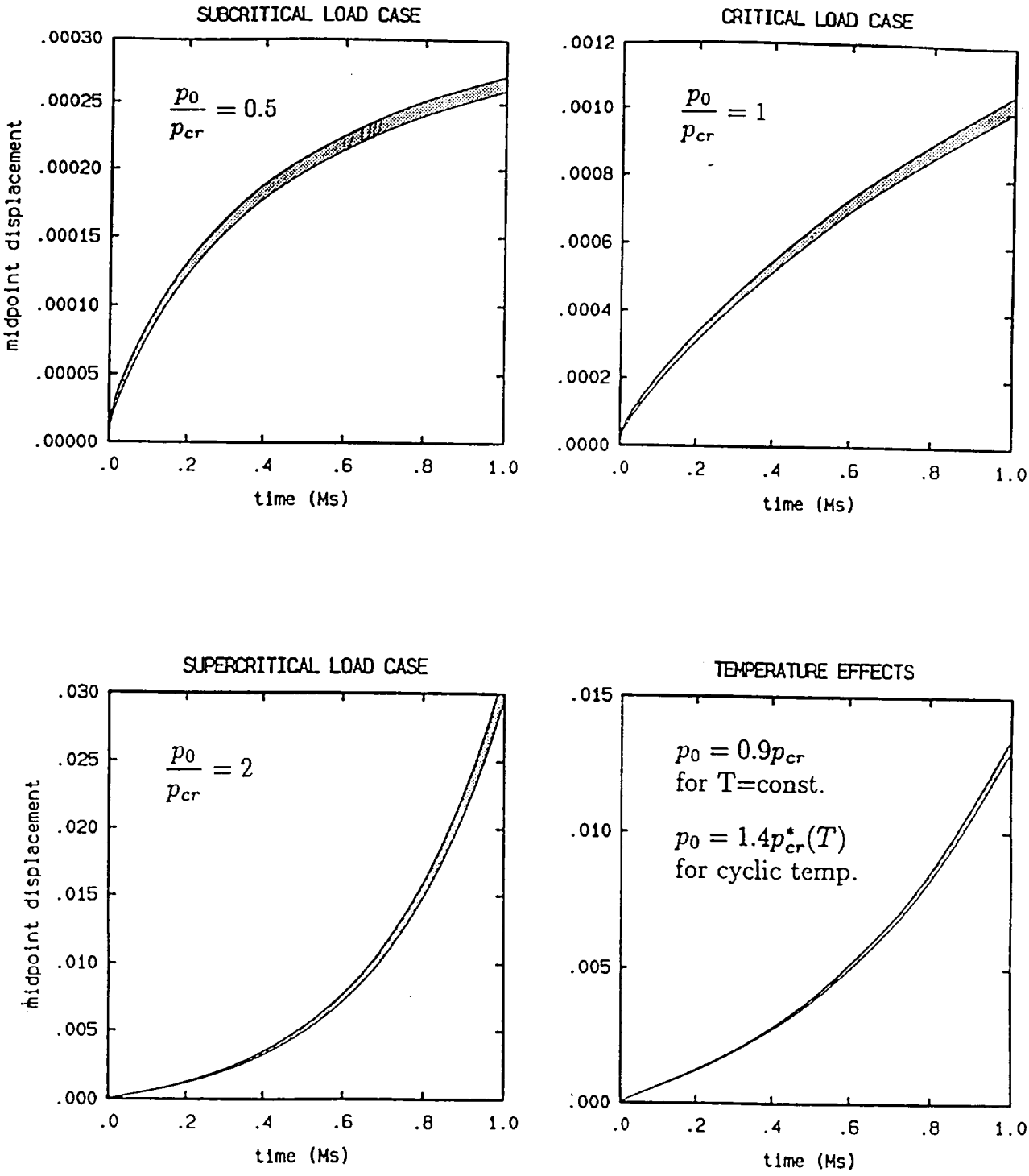
SUBCRITICAL LOAD CASE
$\frac{p_0}{p_{cr}} = 0.5$
midpoint displacement
.00030
.00025
.00020
.00015
.00010
.00005
.00000
.0
.2
.4
.6
.8
1.0
time (Ms)
CRITICAL LOAD CASE
$\frac{p_0}{p_{cr}} = 1$
.0012
.0010
.0008
.0006
.0004
.0002
.0000
.0
.2
.4
.6
.8
1.0
time (Ms)
SUPERCRITICAL LOAD CASE
$\frac{p_0}{p_{cr}} = 2$
midpoint displacement
.030
.025
.020
.015
.010
.005
.000
.0
.2
.4
.6
.8
1.0
time (Ms)
TEMPERATURE EFFECTS
$p_0 = 0.9 p_{cr}$
for T=const.
$p_0 = 1.4 p^*_{cr}(T)$
for cyclic temp.
.015
.010
.005
.000
.0
.2
.4
.6
.8
1.0
time (Ms)

Figure 11

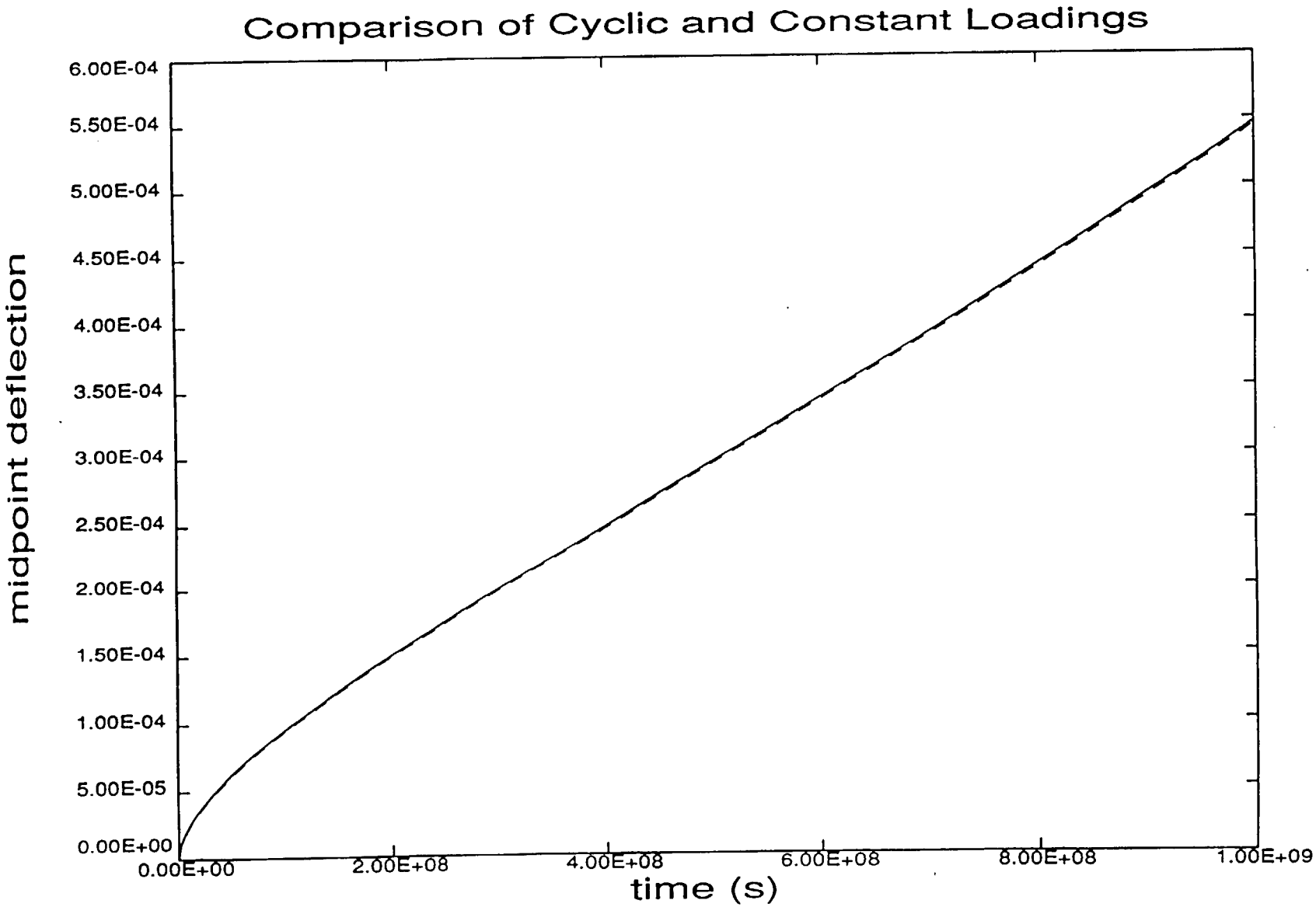
Comparison of Cyclic and Constant Loadings
midpoint deflection
6.00E-04
5.50E-04
5.00E-04
4.50E-04
4.00E-04
3.50E-04
3.00E-04
2.50E-04
2.00E-04
1.50E-04
1.00E-04
5.00E-05
0.00E+00
0.00E+00
2.00E+08
4.00E+08
6.00E+08
8.00E+08
1.00E+09
time (s)

Figure 12

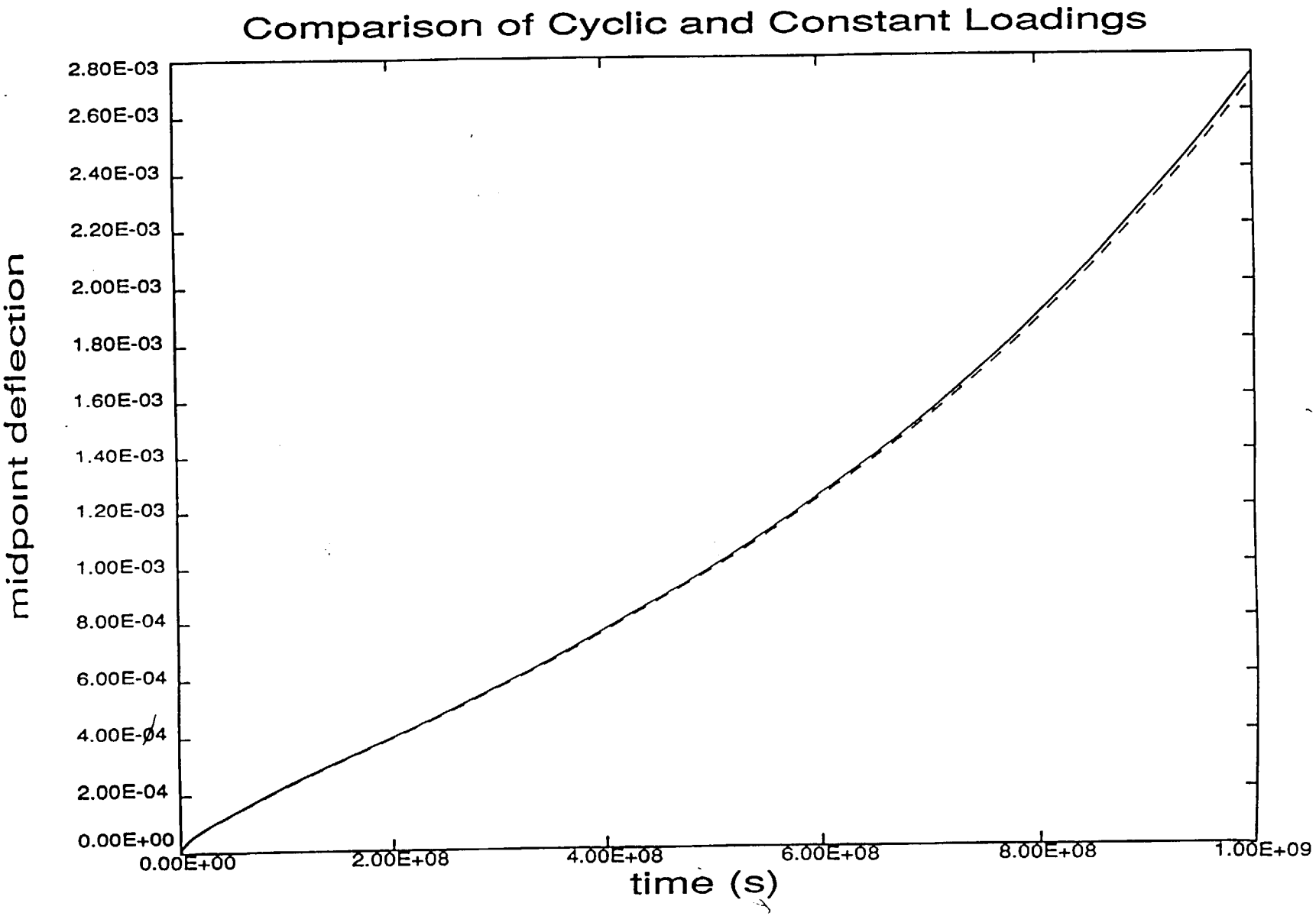
Comparison of Cyclic and Constant Loadings
midpoint deflection
2.80E-03
2.60E-03
2.40E-03
2.20E-03
2.00E-03
1.80E-03
1.60E-03
1.40E-03
1.20E-03
1.00E-03
8.00E-04
6.00E-04
4.00E-04
2.00E-04
0.00E+00
0.00E+00
2.00E+08
4.00E+08
6.00E+08
8.00E+08
1.00E+09
time (s)

Figure 13

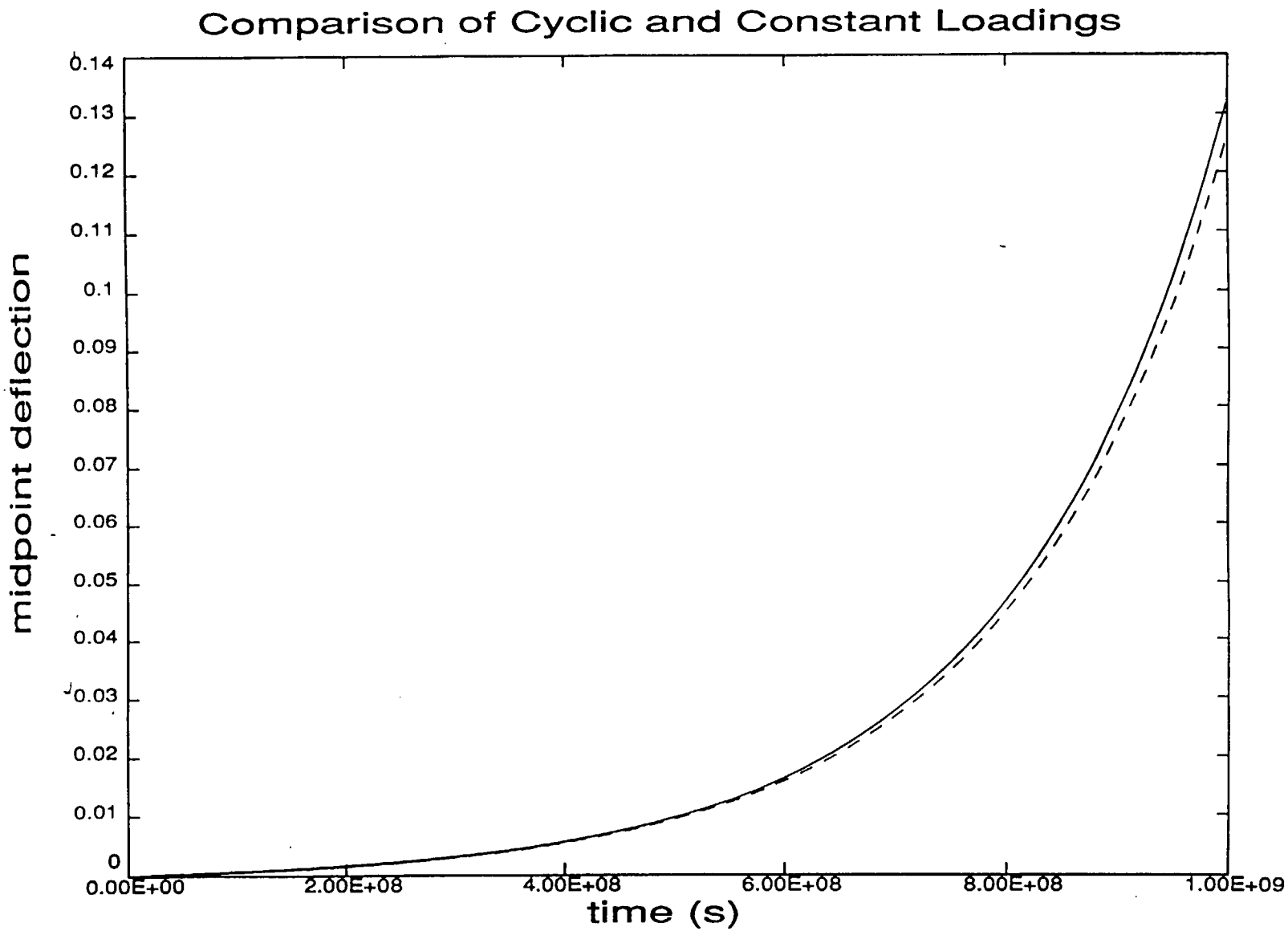
Comparison of Cyclic and Constant Loadings
midpoint deflection
0.14
0.13
0.12
0.11
0.1
0.09
0.08
0.07
0.06
0.05
0.04
0.03
0.02
0.01
0
0.00E+00
2.00E+08
4.00E+08
6.00E+08
8.00E+08
1.00E+09
time (s)

Figure 14

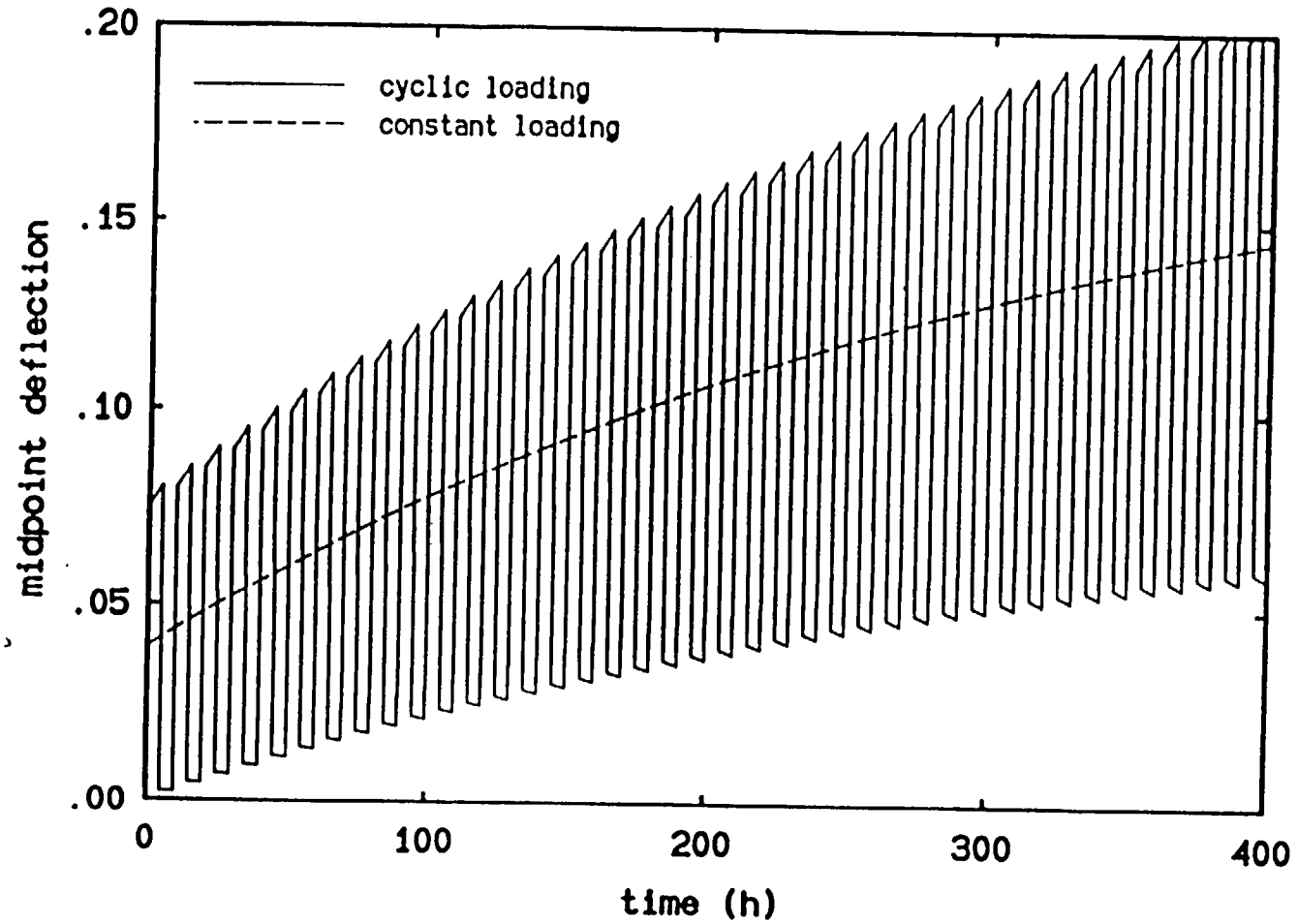
.20
.15
.10
.05
.00
midpoint deflection
cyclic loading
constant loading
0
100
200
300
400
time (h)

Figure 15

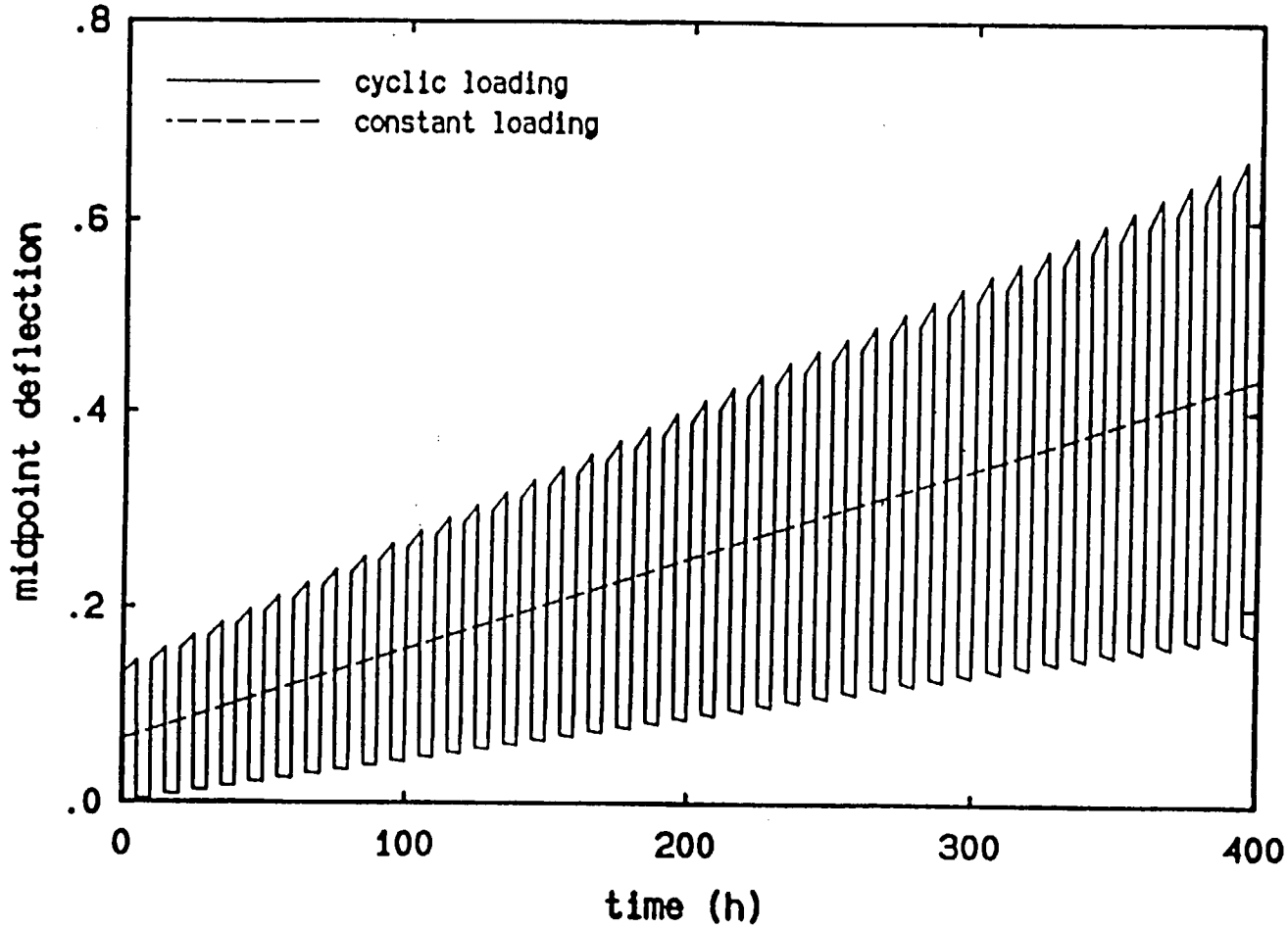
cyclic loading
constant loading
midpoint deflection
.0
.2
.4
.6
.8
0
100
200
300
400
time (h)

Figure 16

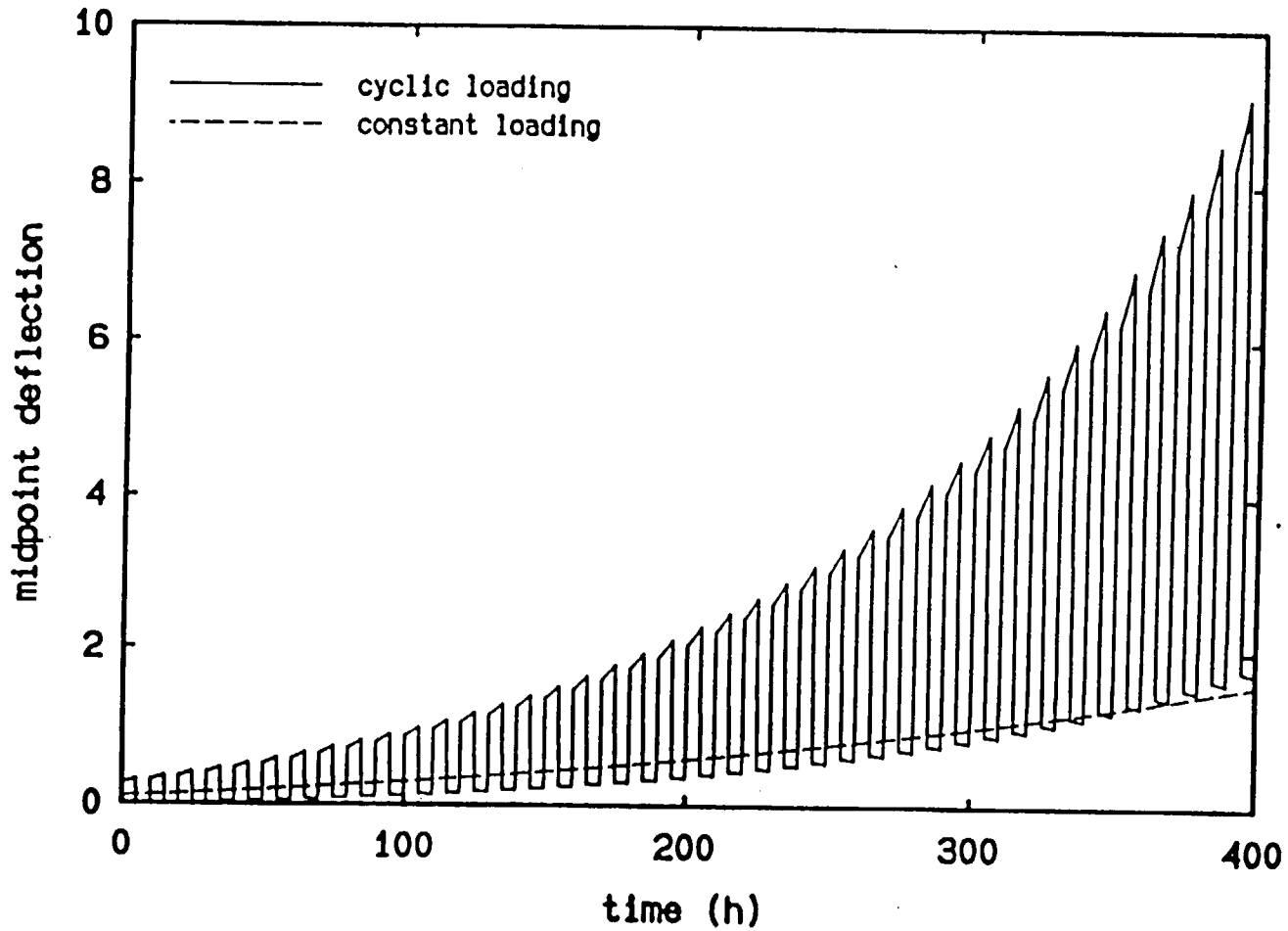
cyclic loading
constant loading
midpoint deflection
time (h)
0
2
4
6
8
10
0
100
200
300
400

Figure 17

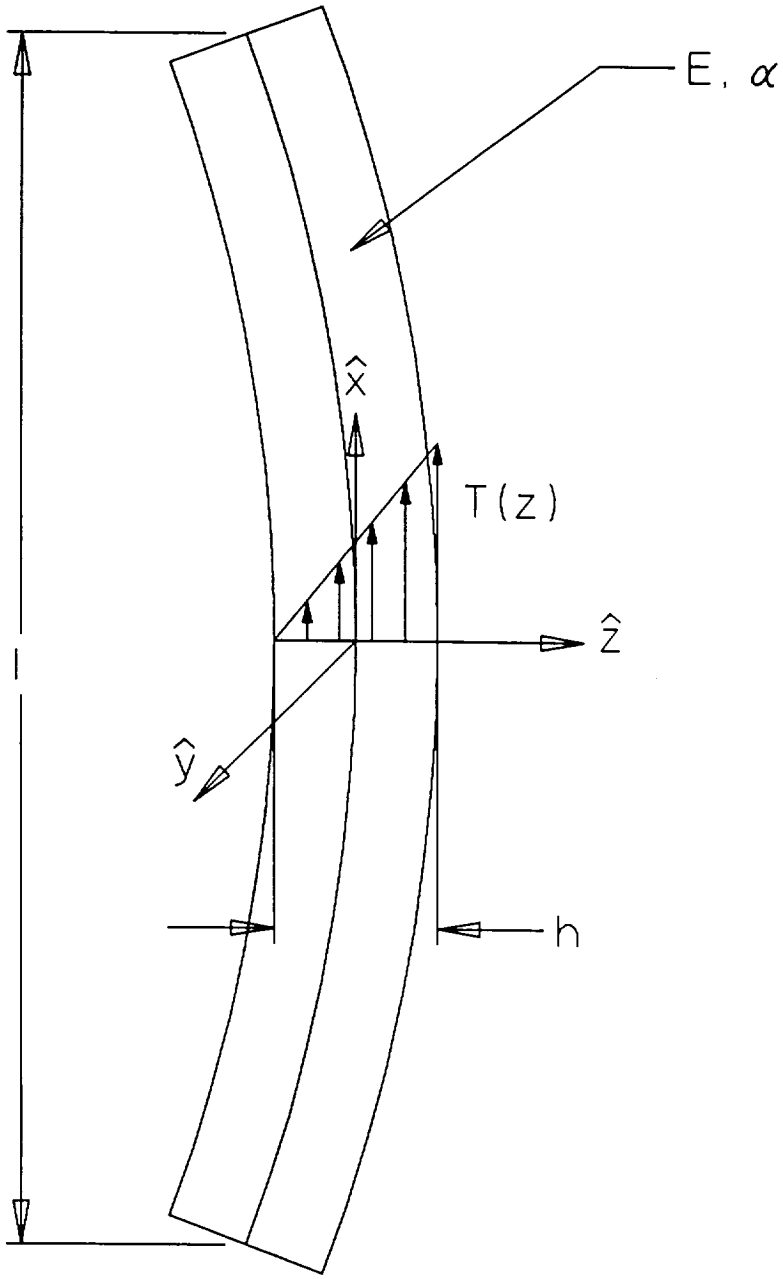

Figure 18 : Elastic Column Under Thermal Gradient

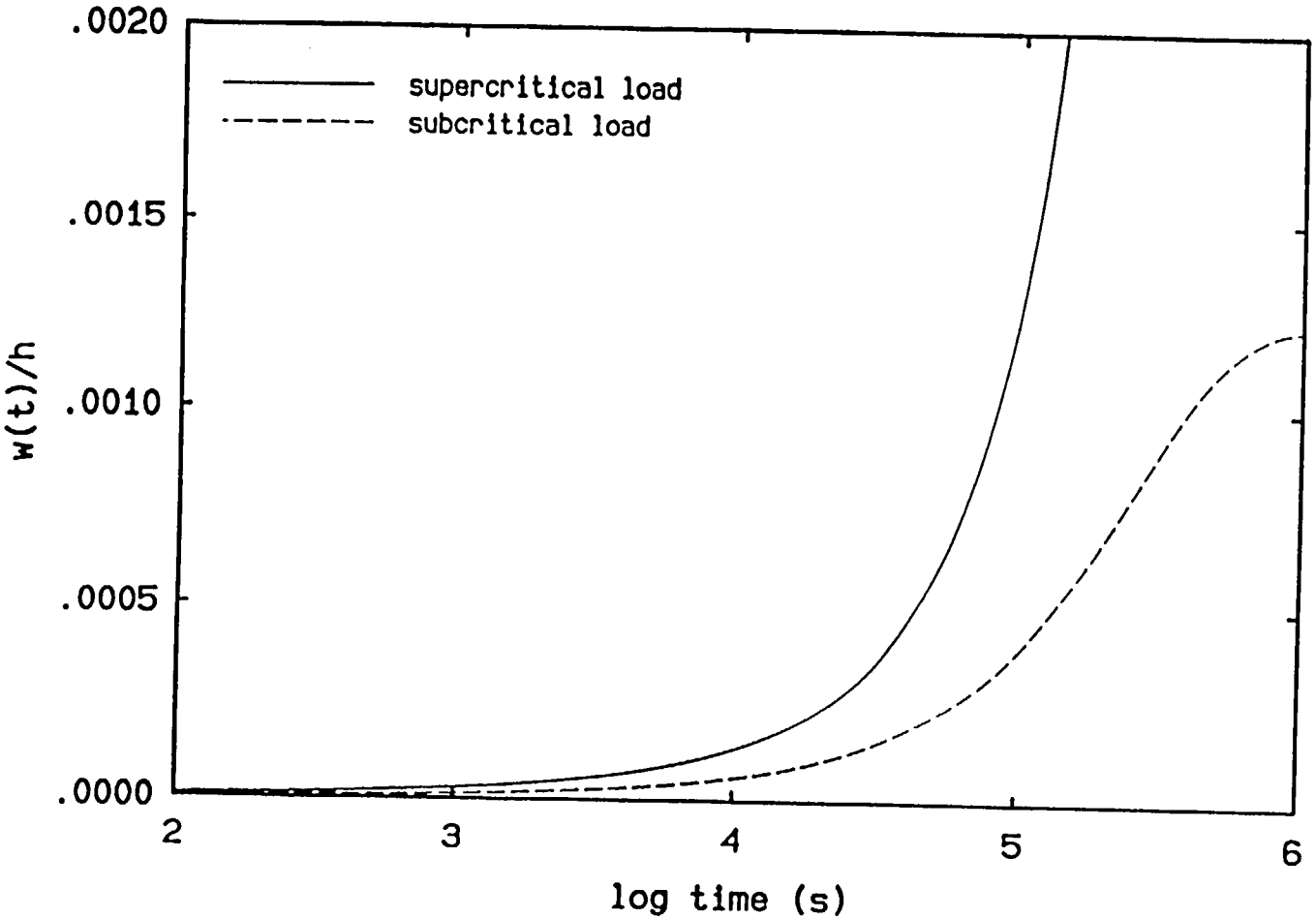
.0020
.0015
.0010
.0005
.0000
w(t)/h
supercritical load
subcritical load
2
3
4
5
6
log time (s)

Figure 19

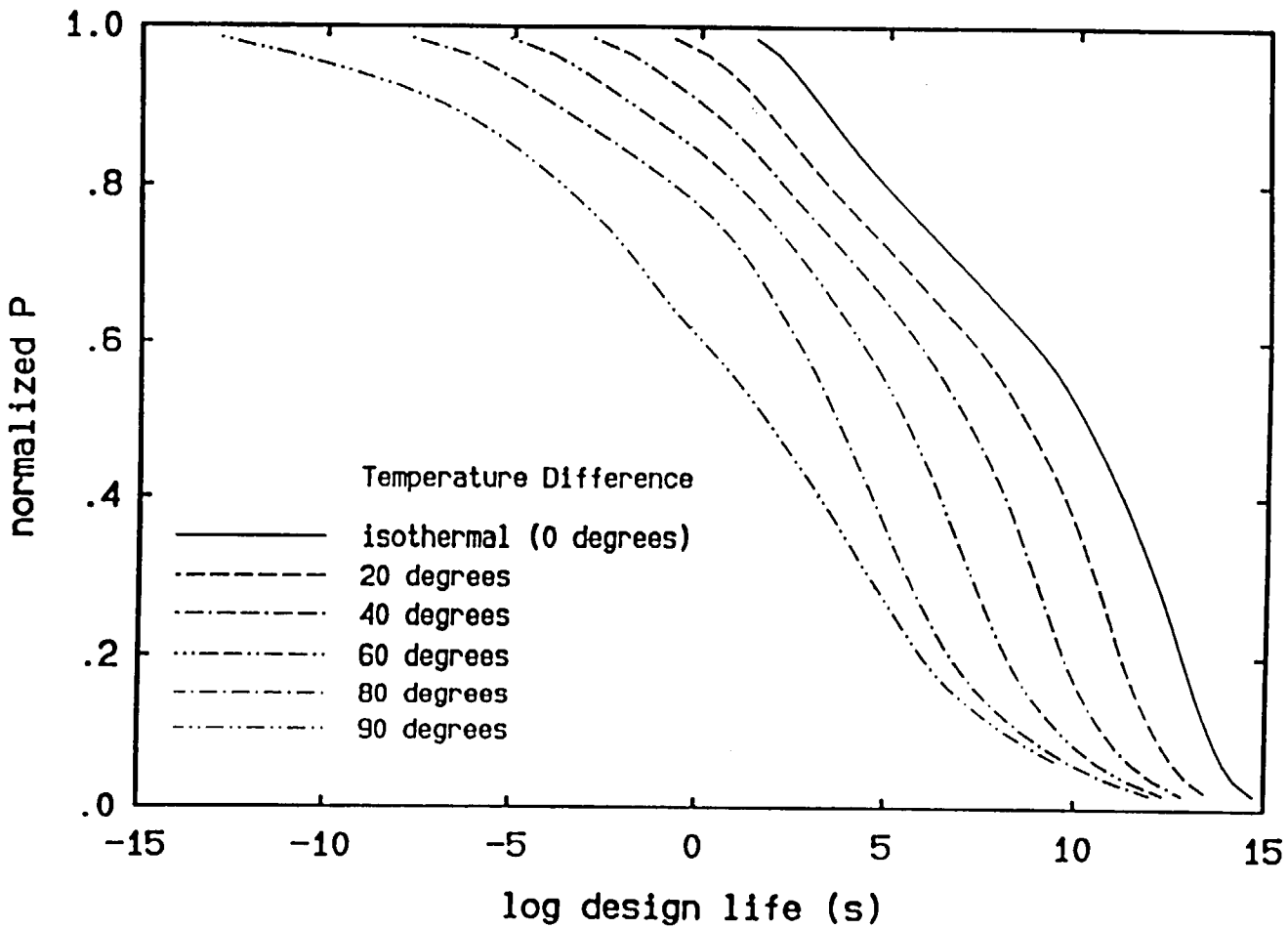
1.0
.8
.6
.4
.2
.0
normalized P
Temperature Difference
isothermal (0 degrees)
20 degrees
40 degrees
60 degrees
80 degrees
90 degrees
-15
-10
-5
0
5
10
15
log design life (s)

Figure 20

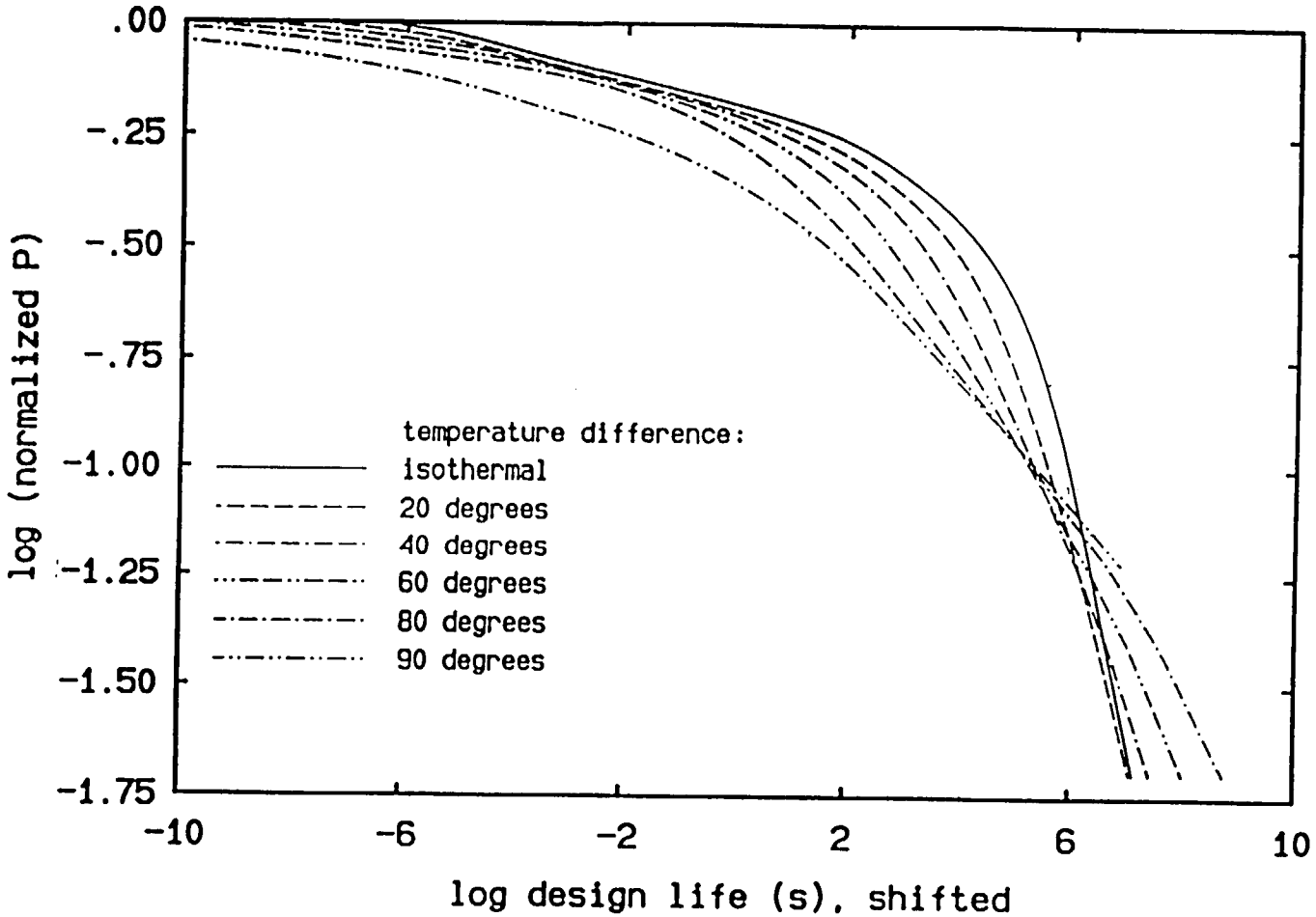
.00
-.25
-.50
-.75
-1.00
-1.25
-1.50
-1.75
log (normalized P)
temperature difference:
isothermal
20 degrees
40 degrees
60 degrees
80 degrees
90 degrees
-10
-6
-2
2
6
10
log design life (s), shifted

Figure 21